CONFIDENTIAL

NASA TECHNICAL MEMORANDUM

UB
NASA TM X-1407

HEAT-TRANSFER AND PRESSURE MEASUREMENTS OBTAINED DURING LAUNCH AND REENTRY OF THE FIRST FOUR GEMINI-TITAN MISSIONS AND SOME COMPARISONS WITH WIND-TUNNEL DATA

by Richard M. Rapp

Manned Spacecraft Center
Houston, Texas

NATIONAL AERONAUTICS AND SPACE ADMINISTRATION • WASHINGTON, D. C. • AUGUST 1967

CONFIDENTIAL

NASA Technical Memorandum X-1407

HEAT TRANSFER AND PRESSURE MEASUREMENTS OBTAINED DURING LAUNCH AND REENTRY OF THE FIRST FOUR GEMINI-TITAN MISSIONS AND SOME COMPARISONS WITH WIND TUNNEL DATA

By Richard M. Raper

August 1967

ERRATA

NASA Technical Memorandum X-1407

HEAT TRANSFER AND PRESSURE MEASUREMENTS
OBTAINED DURING LAUNCH AND REENTRY
OF THE FIRST FOUR GEMINI-TITAN
MISSIONS AND SOME COMPARISONS
WITH WIND TUNNEL DATA

By Richard M. Raper
August 1967

Page 59: Figure 24 has been redrawn as shown below.

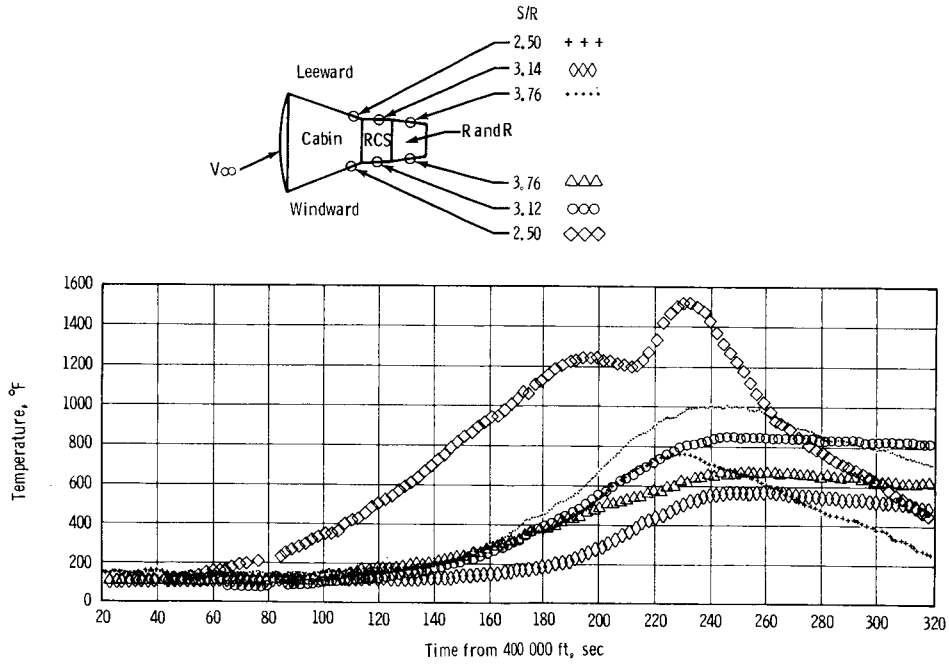

Figure 24. - Gemini II reentry surface thermocouple temperature histories.

Issued 9-30-68

NASA-Langley, 1968

ADDENDUM

NASA Technical Memorandum X-1407

HEAT TRANSFER AND PRESSURE MEASUREMENTS OBTAINED DURING LAUNCH AND REENTRY OF THE FIRST FOUR GEMINI-TITAN MISSIONS AND SOME COMPARISONS WITH WIND TUNNEL DATA

By Richard M. Raper
August 1967

Page 12: This addendum should follow the last sentence of the first complete paragraph.

As an example of the breakdown of the terms of the flight heating-rate calculation, consider the sensor on the RCS windward side at S/R = 3.12. In figure 21(b) a heating rate of 5.1 Btu/ft^2-sec at 240 sec is indicated; this rate corresponds to a surface temperature of 840 °F (fig. 24). At this time the beryllium surface temperature is increasing at the rate of 2.16 deg/sec, corresponding to a rate of energy storage per unit surface area of 3.86 Btu/ft^2-sec. The associated radiation heat loss terms to the surroundings and to the internal structure are 1.22 Btu/ft^2-sec and 0.06 Btu/ft^2-sec, respectively. Although the radiant heat transfer term is a significant element of the heat balance, it is not predominant in this case. At t = 230 sec, a windward side sensor (S/R = 0.250) illustrates a case in which the radiation term dominates. A temperature maximum at this time is shown in figure 24. Thus, the rate of storage term is zero and the entire heat flux rate indicated in figure 21(a) at this time is determined from the radiation terms.

NOTICE

An attempt has been made in this report to give a representative presentation of the aerothermodynamic results of the first four Gemini-Titan missions. However, it was impossible to include all the data and complete details of the data analysis. More detailed information data analysis equations, properties and constants, and additional entry data are available in tabulations from the Central Metric Data Files, NASA Manned Spacecraft Center. The following publications are available.

1. GT-2 Flight Test Data — Heat Transfer. This report contains equations and properties used in data reduction, sensor locations, tabulations of temperature and heating-rate histories, and machine plots of surface heating rates. Twenty-nine sensor locations are included.

2. GT-3 Flight Test Data — Heat Transfer. This report contains tabulations of temperature and heating-rate histories and machine plots of surface heating rates. Five sensor locations are included.

Date _____

TO: Central Metric Data Files
NASA Manned Spacecraft Center
Houston, Texas 77058

Please send a copy of GT-2 Flight Test Data-Heat Transfer (Unclassified) ☐

Please send a copy of GT-3 Flight Test Data-Heat Transfer (Unclassified) ☐

_____
Name of Organization

_____
Street number

_____
City and State Zip Code

Attention*: Mr. _____

Title _____

*To whom copy No. _____ of the TM was issued

Date _____

TO: Central Metric Data Files
NASA Manned Spacecraft Center
Houston, Texas 77058

Please send a copy of GT-2 Flight Test Data-Heat Transfer (Unclassified) ☐

Please send a copy of GT-3 Flight Test Data-Heat Transfer (Unclassified) ☐

_____
Name of Organization

_____
Street number

_____
City and State Zip Code

Attention*: Mr. _____

Title _____

*To whom copy No. _____ of the TM was issued

NASA TM X-1407

HEAT-TRANSFER AND PRESSURE MEASUREMENTS OBTAINED DURING LAUNCH AND REENTRY OF THE FIRST FOUR GEMINI-TITAN MISSIONS AND SOME COMPARISONS WITH WIND-TUNNEL DATA

By Richard M. Raper

Manned Spacecraft Center
Houston, Texas

NATIONAL AERONAUTICS AND SPACE ADMINISTRATION

ABSTRACT

Spacecraft afterbody heating data are presented from measurements made during launch of the first four Gemini-Titan missions, and reentry of the second, third, and fourth missions. Pressure data obtained during launch and reentry of the Gemini II mission are also given.

Heat-transfer data obtained during launch showed that flow over the entire spacecraft was turbulent or transitional when highest heating rates occurred.

Over the windward side of the reentry configuration, heat-transfer rates were in satisfactory agreement with flat-plate theories. Over the leeward side, laminar reentry data showed a minus three-fourths dependence on the reference Reynolds number. Transition to turbulent flow over the spacecraft during reentry occurred in several stages. Transition over the entire leeward side occurred first, followed by transition over the windward side of the reentry control system and the rendezvous and recovery section. Transition over the windward side of the cabin occurred approximately 20 seconds after transition on the reentry control system and the rendezvous and recovery section.

CONTENTS

FIGURES

HEAT-TRANSFER AND PRESSURE MEASUREMENTS OBTAINED DURING LAUNCH AND REENTRY OF THE FIRST FOUR GEMINI-TITAN MISSIONS AND SOME COMPARISONS WITH WIND-TUNNEL DATA*

By Richard M. Raper
Manned Spacecraft Center

SUMMARY

A compilation of representative wind-tunnel heat-transfer and pressure measurements from a number of facilities has been made, and extensive comparisons with flight measurements are shown. These data are interpreted in terms of nondimensionalized pressure distributions, aerodynamic heating rates, and Stanton numbers. The correlated experimental results are compared with theoretical estimates of local pressure and heat-transfer rates.

INTRODUCTION

Relative to the Mercury spacecraft, which was designed to accomplish a ballistic reentry only, the Gemini spacecraft represents a step forward in the design of manned lifting-reentry spacecraft. This spacecraft, as configured for reentry, is a blunt-faced vehicle with a slightly offset center of gravity which permits a hypersonic lift-to-drag ratio of approximately 0.15. Though the Gemini spacecraft is very similar to the Mercury spacecraft in basic shape, it is designed to fly at various angles of attack. Therefore, the quantitative data obtained in the Mercury program are only of limited value with respect to the Gemini Program. However, a qualitative insight into the aerothermodynamic phenomena associated with reentry of vehicles of this type may be gained from previous work concerned with the Mercury spacecraft, some of which is presented herein (refs. 1 to 8).

As a result of design changes made in transition from the Project Mercury program to the Gemini Program, and the need for more information on effects of angle of attack, a wind-tunnel and flight test program was undertaken. Wind-tunnel tests were conducted over a range of Mach numbers from 3.51 to 16.8 in facilities such as the Langley Research Center Unitary Plan Wind Tunnel (ref. 9), Arnold Engineering and Development Center Tunnels B and C (ref. 10), and the Cornell Aeronautical Laboratory

*Title, Unclassified.

4-Foot Shock Tunnel (ref. 11). Flight pressure data were obtained during launch and reentry of the second Gemini-Titan mission spacecraft. Heat-transfer data were obtained during launch of the first mission spacecraft, and during launch and reentry of the spacecraft of the second, third, and fourth missions. This report constitutes the results of an attempt at collection and unification of selected portions of the experimental results, both from ground facilities and flight tests, obtained in the Gemini Program.

SYMBOLS

h	heat transfer coefficient
M	Mach number
$N_{Re, d}$	Reynolds number based on maximum body diameter and free-stream conditions
$N_{Re, x}$	Reynolds number based on surface distance from the stagnation point and local conditions at the edge of the boundary layer
$N_{Re, x}^*$	Reynolds number based on surface distance from the stagnation point and local conditions evaluated at the reference enthalpy
N_{St}^*	reference Stanton number
P	pressure
$\dot{q}$	heat-transfer rate, Btu/ft^2-sec
R	maximum body radius
R^*	minimum body radius
S	surface distance measured from the geometric center of the heat shield
S'	axial distance measured from the leading edge of the rendezvous and recovery section
S^*	surface distance measured from the geometric center of the flat end of the rendezvous and recovery section
α	angle of attack, deg

Subscripts:

L	quantity evaluated at local conditions
T	quantity evaluated at stagnation conditions
2	quantity evaluated at conditions behind normal shock

EXPERIMENTAL CONDITIONS AND DATA TECHNIQUE

In order to assess the aerothermodynamic environment of the Gemini spacecraft, several wind-tunnel and flight tests were conducted. These tests were designed to explore the conditions to which the exit and reentry versions of the spacecraft might be subjected. Shown in figure 1 are sketches of the exit and reentry configurations. Pertinent dimensions (in.) are given for the full-scale vehicle. The two systems for specification of locations on the surface are also illustrated. The first is used for the exit configuration. The axial distance S' is measured from the leading edge of the rendezvous and recovery section (R and R) and is nondimensionalized with respect to the maximum body radius R (R = 45 in. full scale). The system used for the reentry configuration consists of the distances along the surface, measured from the geometric center of the heat shield, and is nondimensionalized with respect to the maximum body radius. The angle of attack is positive in the direction which places the windows on the leeward side of the spacecraft.

Wind-Tunnel Tests

Wind-tunnel tests were conducted in various facilities in order to adequately simulate both exit and reentry flight conditions. Tests of the exit configuration were conducted over a range of angles of attack from -20° to +20°, and the reentry configuration was tested over a -40° to +40° range. Unless indicated otherwise, heat-transfer data were obtained from the transient temperature of the model skin. For all tests of the reentry configuration, the models were supported by a string which was connected to the model on the flat end of the R and R and was parallel to the model centerline. The string was approximately one-half the diameter of the end of the model. A brief description of the various test facilities in which experiments were conducted follows.

Langley Unitary Plan Wind Tunnel (UPWT). - The UPWT is a continuous flow, variable pressure tunnel with a 4- by 4-foot test section. A two-dimensional sliding block nozzle allows variation of the Mach number from 2.3 to 4.65. A detailed description of this facility is available (ref. 12). The test results reported herein were obtained at free-stream Mach numbers of 3.51 and 4.44, with $N_{Re,d} = 2.78 \times 10^6$. Four 0.1-scale models of the spacecraft were tested: heat-transfer and pressure models of the exit configuration, and heat-transfer and pressure models of the reentry configuration.

The heat-transfer models were constructed of type 321 stainless steel, and the skin shells had a nominal thickness of 0.025 inch. The exit heat-transfer model, which

included a portion of the launch vehicle adapter, and the reentry heat-transfer model were instrumented with 146 and 143 thermocouples, respectively. The thermocouples consisted of iron-constantan wire spot welded to the inner surface of the model shells.

The pressure models had thick walls, with 0.093-inch outside diameter tubing soldered into holes flush with the model surface so that the inside diameter of the tube (0.061 in.) formed the orifice. The exit and reentry models were instrumented with 98 and 94 orifices, respectively.

Arnold Engineering and Development Center Tunnels B and C. - Tunnels B and C are both axisymmetric, continuous flow, variable density, hypersonic wind tunnels with 50-inch test sections. A detailed description of both facilities is available (ref. 13). Four 0.1-scale models of the spacecraft were tested: heat-transfer and pressure models of the reentry configuration and heat-transfer and pressure models of the exit configuration. The exit configuration pressure model was tested at Mach number 8, with $N_{Re, d} = 1 \times 10^6$ in Tunnel B, and the other three models were tested in Tunnel C at Mach number 10, with $N_{Re, d} = 0.5 \times 10^6$ to 1.6×10^6.

The heat-transfer models were constructed from 0.025-inch stainless steel. Approximately 140 chromel-alumel thermocouples were spot welded to the inner surfaces of the models, though only 98 could be monitored during a particular test. The pressure models were instrumented with 99 pressure orifices.

Cornell Aeronautical Laboratory 48-Inch Shock Tunnel. - The tunnel has a constant-area reflected-shock tube which processes air to conditions suitable for supplying a convergent-divergent hypersonic nozzle. The shock-processed air is expanded through one of a series of nozzles to the desired test conditions. A complete description of this facility is available (ref. 14). Two 0.07-scale models of the spacecraft were tested. These were heat-transfer and pressure models of the reentry configuration. Each model was tested at Mach numbers 13 and 16.8, with $N_{Re, d} = 3.2 \times 10^5$ and 0.5×10^5, respectively.

Both the heat-transfer and the pressure models used in this test were constructed of brass. Heat-transfer rates were determined from the transient temperature of thin platinum strips (approximately 0.1μ) which were deposited on pyrex substrates (mounted on the model flush with the surface). Model surface static pressures were measured with pressure transducers which used piezoelectric crystals as sensing elements. Their small size permitted installation within the model, close to the orifice.

Flight Tests

The Gemini aerothermodynamic flight test program was composed of the first four Gemini-Titan (GT) missions. The first flight (GT-1) was unmanned and was not recovered. Its primary purpose was to provide verification of the structural integrity and compatibility of the launch vehicle and spacecraft, and to determine the exit heating conditions on the spacecraft. The second flight (GT-2) was also unmanned, but the

spacecraft was recovered. The major objectives of this mission were to demonstrate the basic structural integrity of the unit throughout the flight environment and to verify the adequacy of the reentry heat protection system under the most severe conditions. The third and fourth missions (GT-3 and GT-4, respectively) had the acquisition of aerothermodynamic data as minor objectives only.

Configuration and thermal protection system. - The configurations of the exit and reentry versions of the Gemini spacecraft are shown in figure 1. The exit configuration consists of the spacecraft, oriented conical-section forward, and a spacecraft-to-launch-vehicle adapter which is attached to the blunt end. Prior to reentry, the adapter section is jettisoned, leaving only the blunt-faced reentry module.

The Gemini spacecraft thermal protection system consists of a blunt-ablation heat shield over the forebody and René 41 and beryllium heat shields over the afterbody. The forebody heat shield is composed of a silicone elastomer contained in a phenolic honeycomb core (3/16-in. cell size), with a resultant specific weight of 54 lb/ft^3. On the afterbody, the cabin section is covered with 0.016-inch corrugated René 41 shingles. The substructure in this area is insulated from the outer skin by a 1.5-inch layer of 7 lb/ft^3 specific weight refractory-fiber insulation. The reentry control system (RCS) is covered with beryllium plates, the thickness of which varies from 0.28 inch on the windward side to 0.09 inch on the leeward side. A 1.0-inch layer of 12 lb/ft^3 specific weight refractory-fiber insulation is located between the outer skin and the underlying structure. The outer surface of the R and R also consists of beryllium plates, with thickness varying from 0.20 inch on the windward side to 0.09 inch on the leeward side. A 1.0-inch thickness of 7 lb/ft^3 specific weight insulation of the type just described is used to insulate the substructure.

Instrumentation. - During ascent and reentry of the spacecraft, surface temperatures on the cabin section were measured by chromel-alumel thermocouples spot welded to the inside of the peaks of the corrugations. Temperatures on the beryllium plates were measured from a somewhat different arrangement. In this case, the thermocouples were welded to small washers made of 0.016-inch René 41 which were riveted to the inside surface. The rivets were fabricated from monel alloy and were 0.13 inch in diameter. This method of installation is believed to yield satisfactory measurements, since the mass of the skin is large relative to the mass of the thermocouple hardware. The first two spacecraft of the Gemini Program were instrumented with a large number of thermocouples (28 and 29, respectively). The third and fourth flights carried only five and eight thermocouples, respectively, since the data were intended mainly to substantiate data obtained during earlier missions. Other thermocouples were imbedded in the ablation heat shield, but this report will consider only those on the metal afterbody of the spacecraft. The thermocouple data were telemetered at 1.25-second intervals.

Surface pressures were measured at eight locations during launch and reentry of Gemini II spacecraft. The transducers on the leeward side of the reentry configuration had a range of 0 to 0.2 psia, and those on the windward side had a range of 0 to 0.8 psia.

Calculation of heating rates. - Afterbody heating rates were machine-calculated from the transient thermal response of the skin. A second-degree polynomial was

constructed by the Least Squares technique using 21 data points (10 points on each side of the time under consideration) from the flight telemetry data. The change of temperature with time is given by the first derivative of the polynomial. The temperature distribution through the wall of the spacecraft is found by solving eight simultaneous one-dimensional finite difference equations which represent the differential equations defining transient temperatures (at each selected node) through the wall. The input heating rate at the outside surface may then be calculated. It is the sum of the rate at which heat is stored in the outer skin, the rate at which heat is reradiated from the external surface of the outer skin, the rate at which heat is radiated to the interior of the wall, and the rate at which heat is conducted to the interior of the wall. The external surface emissivity was assumed to be 0.9. The effect of the thermal mass of the thermocouple, or any of its associated hardware, was not accounted for. However, calculations performed for similar thermocouple installations on the Mercury spacecraft indicate the resulting error in heating rate to be less than 10 percent (ref. 8).

RESULTS AND DISCUSSION

Exit Data

Wind-tunnel test conditions for the exit configuration were chosen to simulate Mach numbers and Reynolds numbers expected during the corresponding phase of the flight. Pressure and heat-transfer data in the plane of symmetry of the vehicle, obtained during flight and in wind-tunnel tests, are compared as follows.

Wind-tunnel data. - Results of wind-tunnel tests of the pressure model of the exit configurations and comparisons with the tangent-cone theory are shown in figure 2. The data are presented as the ratio of the local pressure to the stagnation pressure behind a normal shock wave. The solid lines represent a fairing of the data for each test Mach number, and the broken lines give the levels of the estimates. Sufficient data were not obtained to assess the dependence of the pressure distribution on the free-stream Reynolds number at the lower Mach numbers, but the tests at $M = 8$ indicate no significant variation over the range for which these tests were conducted. The pressure distribution over the cabin and adapter sections is strongly dependent on Mach number. The maximums in local pressure noted on the adapter near $S'/R = 3.72$ are caused by the presence of the circumferential ring at $S'/R = 3.78$ (ref. 4). At $\alpha = 0^\circ$ the tangent-cone estimates are reasonably successful for use in predicting the undisturbed level of the pressures on the adapter section. A comparison of the data and estimates on the cabin section, however, suggests a pronounced upstream effect on the R and R and the RCS section. Thus, although the Mach number trend is given by the tangent-cone theory in this region, the pressure levels are only poorly estimated. Introducing a small angle of attack (fig. 2(b)) resulted in an overall increase in the pressure distribution over the windward side.

A distribution of heating rates in the pitch plane of the flat face of the R and R of the exit configuration at $\alpha = 0^\circ$ is presented in figure 3. The local heating rate is divided by the heating rate at the stagnation point of a hemisphere of the same radius and at the same flow conditions. The position on the flat face is denoted by the distance from the geometrical center S* divided by the radius of the face R*. Also shown, for purposes of comparison, are data obtained on flat-faced cylinders for a range of

Mach numbers from 2.0 to 13.8 (ref. 15). These data were obtained in wind-tunnel and rocket-powered free-flight tests. The solid line gives a theoretical laminar distribution for the flat face by the method of Stine and Wanlass (ref. 16). The data are in satisfactory agreement with those obtained by the investigators just mentioned. For values of $S^*/R^* > 0.5$ the data fall below the theoretical curve.

Shown in figure 4 are the results of wind-tunnel tests of the heat-transfer model of the exit configuration. The data are presented as the ratio of the local heat-transfer coefficient to the stagnation-point heat-transfer coefficient at zero angle of attack with the heat shield forward, with the coefficients at the same M and $N_{Re,d}$ values. The lines represent a fairing of the data for each experimental test Mach number. As was the case for the pressure distribution over the exit configuration, the heat-transfer distribution is strongly dependent on the free-stream Mach number. The circumferential ring on the adapter ($S'/R = 3.78$) creates a region of high heating at the low Mach numbers. However, at $M = 10$ a much weaker effect of the ring is evident in both heat-transfer and pressure data. Overall increases in the heating over the windward side resulted from increasing the angle of attack (fig. 4(b)). Analysis of the data in terms of Stanton numbers and Reynolds numbers, and comparison with flat-plate theory, indicated that flow over the entire spacecraft was turbulent or transitional at the low Mach numbers and laminar at $M = 10$. This analysis is presented in the next section. Thus, differences between the distributions shown in figure 4 are attributed to both Mach number and transitional effects.

Flight data. - A nominal Gemini launch trajectory through first-stage burnout is shown in figure 5. Maximum heating rates were generally attained approximately 105 seconds after lift-off, which corresponds to an altitude of 86 000 feet and a velocity of 3100 ft/sec. The nominal trajectory in terms of the Mach number and Reynolds number is shown in figure 6. Also shown are the wind-tunnel test conditions which are related to the flight conditions through the test Mach number and Reynolds number. In terms of these parameters, maximum heating conditions were generally attained at the point denoted by the asterisk, which is at a lower Mach number and higher Reynolds number than any of the test conditions.

Pressure distributions obtained in wind-tunnel tests of the exit configuration indicated that the nondimensionalized surface pressure is primarily a function of the free-stream Mach number, and is not significantly affected by the Reynolds number over the range of conditions for which significant heating was obtained. Figure 7 shows a comparison of the wind-tunnel pressure distribution at $\alpha = 0°$ and flight pressure measurements obtained during the exit phase of the GT-2 mission. The data are presented as the ratio of the local pressure to the stagnation pressure behind a normal shock. The lines are a fairing of wind-tunnel data obtained at the indicated Mach number, and the symbols represent flight measurements obtained at the point in the trajectory where the Mach number was equal to a wind-tunnel test Mach number. Agreement of the wind-tunnel and flight data is satisfactory on the cabin section. However, the flight data do not follow closely the trend of the wind-tunnel data on the RCS section, though the levels indicated are comparable.

Representative heating-rate histories obtained at several locations over the spacecraft of the GT-2 mission during exit are shown in figure 8. None of the heating rates shown exceeded 1.0 Btu/ft^2-sec. Typical peak heating rates on the R and R and

the RCS compartment were 0.8 Btu/ft^2-sec and 0.5 Btu/ft^2-sec, respectively. The behavior prior to 90 seconds of the heating-rate history presented for the R and R (S'/R = 0.49) is not explained. The cabin section underwent somewhat more severe peak heating rates, 0.9 to 1.0 Btu/ft^2-sec on the forward portion and 0.45 Btu/ft^2-sec at the station furthest aft.

A comparison of heat-transfer coefficient distributions measured in wind-tunnel and flight tests is shown in figure 9. The wind-tunnel measurements were presented earlier (fig. 4), but are repeated here for comparative purposes. The data are presented as the ratio of the heat-transfer coefficient (at the point of interest) to the heat-transfer coefficient at S'/R = 2.34 (on the cabin section). Presentation of the data in this form is employed to retain the general shape of the heating distribution observed in figure 4, and yet avoid referencing the turbulent measurements to a laminar theory. The filled symbols denote data obtained during exit of the Gemini II spacecraft. The shape of the symbol denotes the Mach number, which is the same as that of one of the wind-tunnel tests. The Reynolds number generally was not duplicated. Flight data obtained at M = 10 are not shown because heating rates obtained at this point in the trajectory were either negative or so small that the noise level of the telemetry system was of the same order of magnitude as the measurement. The agreement of the flight and wind-tunnel data is satisfactory over most of the spacecraft.

A correlation of the heating data in terms of N_{St}^* and $N_{Re,x}^*$ for several common locations on the Gemini I, Gemini II, and Gemini III spacecraft is shown in figure 10. The lines labeled laminar-attached and turbulent-attached (figs. 10(a) and 10(b)) represent the theoretical levels of heating on a flat plate subjected to attached flow. The theoretical levels of heating for separated flow on a flat plate are given by the two remaining lines and were taken to be 56 and 60 percent of the attached values for the laminar and turbulent cases, respectively (ref. 16). The filled symbols represent wind-tunnel data which are shown for comparison. Data obtained on the R and R indicate that the flow is initially turbulent, with transition to laminar flow beginning at $N_{Re,d}$ approximately 1.5×10^5. Over the RCS section, transition of the flight data is shown to begin at an $N_{Re,d}$ of about 10^6. A discrepancy among transition Reynolds numbers for the wind-tunnel and flight data was observed. The lines labeled laminar and turbulent represent the theoretical level of heating on a pointed cone (fig. 10(c)). Measurements for the cabin section are generally in agreement with the pointed-cone theory. As suggested in the previous section, wind-tunnel measurements obtained over the entire spacecraft indicate that the flow was either turbulent or transitional at the low Mach numbers and laminar for M = 10. Over the locations for which data are presented, measurements obtained on all flights are in satisfactory agreement with each other. Also, wind-tunnel data were generally substantiated by the flight measurements.

Reentry Configuration Measurements

Wind-tunnel test parameters for the reentry configuration of the Gemini spacecraft were chosen to partially simulate a wide range of conditions encountered during reentry. Afterbody flow separation and transition were of particular interest. Flight

data were obtained during both nominal and maximum heating reentries. Measurements obtained in the plane of symmetry of the vehicle are presented in the following section.

Wind-Tunnel Data

Pressure data. - Pressure distributions over the windward side of the afterbody of the reentry configuration at angle of attack are shown in figure 11. The data fall into two bands, one for $M > 10$ and (a higher one) for $M < 5$. The difference between the levels of the two bands increases with increasing angle of attack. Within the band of high Mach number data, little effect on either Mach number or Reynolds number is noted, except over the RCS section (S/R = 2. 82 to 3. 43). The pressure obtained at the lower Mach numbers, however, decreases with increasing Mach number. Data for the cabin section (S/R = 1. 05 to 2. 82) indicate that the local pressure is strongly dependent upon the angle of attack, particularly in the central region. In this region the pressure measured at each point increases substantially with an increase in angle of attack. Data for the RCS section show that at S/R = 2. 91 the pressure is dependent primarily on the Reynolds number. At other locations on the RCS the data appear to vary with both Reynolds number and Mach number. Wind-tunnel tests of the Mercury spacecraft over a wide range of flow conditions (ref. 5) have shown that the local pressure over the cylindrical section of configurations of this type at $\alpha = 0^\circ$ is strongly dependent on the Reynolds number. The present data indicate that this dependency is reduced when $\alpha > 0^\circ$. The level of the local pressure does not change significantly with angle of attack in the range $10^\circ < \alpha < 20^\circ$. Over the R and R a definite trend of the data with Reynolds number is not immediately apparent. Again, the effect on angle of attack is not appreciable. The level of the pressure distributions over the leeward side of the afterbody of the reentry configuration at this angle of attack (fig. 12) indicates that the flow is separated except for an aft region where partial reattachment may occur, depending on the angle of attack. During tests of the Mercury spacecraft (refs. 1 and 3), the afterbody flow field was qualitatively studied by oil flow, schlieren, and shadowgraph techniques. Quantitative pressure data were also obtained. It was found that for this shape the flow separated from the afterbody when the angle of attack was such as to place the surface at a reentry angle of more than 10° from the free stream. The level of the surface pressure associated with these regions of separated flow was found to be less than 2 percent of the stagnation value. Over the cabin and RCS sections of the present configuration, the pressures do not exceed 2 percent of the stagnation value. Little effect on angle of attack is noted over the range for which data are shown. Thus, the present data substantiate the fact that the level of pressure on the leeward side of blunt bodies of this type tends to be about 1 to 2 percent of the stagnation value, independent of the flow conditions, angle of attack, and configuration details (ref. 17). Over the leeward side of the R and R the pressure increases significantly with decreasing angle of attack. For a given angle of attack the level of pressure is dependent on both Mach number and Reynolds number.

Heat-transfer data. - Distributions of heat-transfer rate over the windward side of the reentry configuration afterbody at angle of attack (fig. 13) exhibit some of the characteristics observed in the pressure distributions. At the lowest angle of attack, heat-transfer rates over the cabin section are less than 10 percent of the $\alpha = 0^\circ$ stagnation-point value. These rates increase to approximately 20 percent at $\alpha = 20^\circ$. Heating rates over the RCS section tend to depend strongly on the flow conditions, particularly at lower angles of attack. This is attributed to the complex interaction of the

approaching cabin-section flow field with the compression waves which are generated by the cylindrical RCS section. The heating over the RCS section would be expected to exceed that measured on the cabin section because this surface is inclined forward to the free-stream flow. However, it may be seen in figure 24 that the high heat-transfer rate measurements over the RCS section were obtained in a turbulent flow, whereas those for the cabin section were obtained in a laminar flow. The RCS distribution is not strongly affected by changes in angle of attack, and the peak value was roughly 50 percent of the stagnation-point value. These measurements were obtained at the highest test Reynolds number. Heating rates over the windward side of the R and R show little variation with either test conditions or angle of attack. Peak values were approximately 25 percent of the stagnation-point value.

Heat-transfer rate distributions over the leeward side of the reentry configuration afterbody at angle of attack are shown in figure 14. Over the forward portion of the cabin the heating rates were approximately 3 percent of the stagnation-point value, and increased to as much as 8 percent further aft. As was noted for the leeward side pressure distribution, flow over the aft area of the configuration is dependent on both Reynolds number and the Mach number. At the extreme aft end of the R and R, the level of heating is 28 percent of the stagnation-point value at the lowest angle of attack and highest Reynolds number. At $\alpha = 20^\circ$ the peak is 14 percent. Thus, at low angles of attack, the level of heating on the leeward side of the R and R may exceed that on the windward side for large Reynolds numbers.

Flight Data

Measurements of heat-transfer rates and surface pressures were obtained over a wide range of free-stream conditions during reentry of the second, third, and fourth Gemini spacecraft. Altitude and velocity as a function of the time from 400 000 feet for each spacecraft during reentry are shown in figure 15. The Gemini II mission, as was stated before, was unmanned and simulated an abort just prior to orbital insertion. The relatively steep flight-path angle resulted in heating rates over the vehicle of close to maximum design values. A continuous rolling maneuver was executed during most of the reentry to cancel the lift force, giving a near ballistic trajectory. The Gemini III spacecraft flew a lifting reentry which was considerably less severe in terms of peak heating rate than a nominal reentry. The Gemini IV mission was terminated with a near nominal rolling reentry, falling between the two earlier missions in terms of peak heating rates. These trajectories, shown in figure 16, are in terms of Mach number and Reynolds number. The figure also shows test conditions for which wind-tunnel data for the reentry configuration were obtained. These test conditions are related to the flight conditions through the Mach numbers and Reynolds numbers, since the free-stream conditions occurring in flight are not duplicated in the wind tunnel.

Angle of attack. - Each of the three Gemini spacecraft considered here had different aerodynamic trim characteristics. Shown in figure 17 is the variation of the estimated trim angle of attack with Mach number during each reentry. The inertial guidance system data were used to compute the spacecraft angle of attack. The center of gravity of the Gemini II, Gemini III, and Gemini IV vehicles was displaced in the pitch plane from the centerline of the spacecraft 1.96, 1.43, and 1.58 inches, respectively. As is shown in the figure, the Gemini III spacecraft flew at a considerably lower angle of attack than either the Gemini II or Gemini IV. The Gemini II spacecraft

center of gravity was offset the greatest and trimmed at an angle of attack of approximately 15° during the period of significant aerodynamic heating.

Another indication of the angle of attack during reentry may be obtained from visual inspection of the heat shield after recovery of the spacecraft. Surface ablation leaves a distinct pattern of material flow lines which emanate from a relatively large stagnation region (fig. 18). These may be taken as indicative of streamlines of airflow over the body. The apparent stagnation-point location may be found by placing strings along these streamlines in such a manner that the point of intersection is determined. This point of intersection of the streamlines should approximate the stagnation-point location, because the angle of attack calculated as described above was fairly constant during the period of significant heating and cooling of the outer surface of the heat shield. Heat-shield stagnation-point locations for the Gemini II, Gemini III, and Gemini IV spacecraft measured as just described are shown in figure 19. The locations are plotted against angles of attack, which were taken from the preceding figure at M = 15. Also shown, for comparative purposes, are the stagnation-point locations determined from wind-tunnel pressure distributions over the heat shield, and the stagnation-point location as given by the modified Newtonian theory. Agreement of the postflight measured stagnation-point location with the wind-tunnel data is satisfactory. As expected, the movement of the flight and wind-tunnel stagnation points with angle of attack was considerably more gradual than predicted by the Newtonian theory.

Pressure measurements. - A comparison of pressure measurements on the afterbody surface obtained during the Gemini II spacecraft reentry with wind-tunnel measurements is shown in figure 20. The data are presented in terms of the local pressure divided by the calculated pressure behind a normal shock versus the free-stream Mach number. The lines are a fairing of the flight data, and the broken portions indicate interpolation through a data loss period. (The rail symbol denotes the amount by which a ±1 percent of full-scale error in the measurement of the local pressure would change the pressure ratio.) As would be expected, the ratio is most sensitive to error when the pressure is low, that is, at high Mach numbers. The other symbols represent wind-tunnel data obtained at $\alpha = 15^\circ$. Over the cabin section the flight and wind-tunnel data were generally in satisfactory agreement. For the RCS section, the pressure measured during flight in the forward region was above the pressure shown by the wind-tunnel data. Over the central area, the trend was reversed. Though the levels of the wind-tunnel and flight data differ somewhat, the trends with Mach number are similar for both locations. The disagreement in level of the data was attributed to the difference of Reynolds number between the wind-tunnel and flight measurements. Wind-tunnel and flight pressure data over the leeward side of the spacecraft (fig. 20(b)) were in satisfactory agreement, and the level of the measurements is indicative of a completely separated flow. Surface pressures in excess of 2 percent of the total pressure were obtained at only one point (S/R = 3.14), and then only over a short Mach number interval.

Heat-transfer data. - Some selected heating-rate histories measured over the Gemini II spacecraft during reentry are shown in figure 21. The data are presented in terms of the absolute heating rate versus time from 400 000 feet. Measurements obtained on the windward side of the cabin indicate peak heating rates ranging from 7.2 to 11.7 Btu/ft^2-sec. The shape of the curves for the cabin section suggests that the peak laminar heating rates occurred at approximately 190 seconds (the calculated laminar stagnation-point heating rate also peaked at that time), followed by the turbulent peaks

at 220 to 230 seconds, depending on location. The behavior of the curve of S/R = 1.41 is observed to differ in character from those for other locations on the cabin section, possibly as a result of its proximity to the heat-shield shoulder. Peak heating rates on the windward side of the RCS section ranged from 9 to 21.9 Btu/ft^2-sec. These curves are characterized by maximums which occurred at about 210 seconds, slightly before the turbulent peaks observed on the cabin. Considerably lower heating rates were observed for the R and R; peaks ranged from 5.2 to 6.6 Btu/ft^2-sec. Peak heating rates over the leeward side of the spacecraft ranged from 1.7 Btu/ft^2-sec on the cabin, and 4.1 Btu/ft^2-sec on the RCS, to 8.6 Btu/ft^2-sec on the R and R. It is of interest to note that heating rates on the leeward side of the R and R exceeded those on the windward side, a trend which was noted in the wind-tunnel data for large Reynolds numbers.

Representative windward-side heating-rate histories measured during the Gemini III and Gemini IV spacecraft reentries are shown in figures 22 and 23, respectively. As would be expected, the level of heating was considerably lower than that obtained during reentry of the Gemini II spacecraft. Also, the curves do not exhibit any second peaks of the type which would appear to indicate transition from laminar to turbulent flow. The calculated laminar stagnation-point heating rate for the Gemini III spacecraft peaked at 358 seconds, and at 319 seconds for the Gemini IV. The length of the period over which significant heating was encountered was 425 seconds for the Gemini III spacecraft reentry, and 280 seconds for the Gemini IV spacecraft reentry. For comparison, this time period for the Gemini II spacecraft reentry was approximately 230 seconds. As an illustration of the character of the basic thermocouple data, a few selected surface-temperature measurements taken during the reentry of the Gemini II spacecraft are given in figure 24. Comparison of figures 21 and 24 shows the inferred heating rates in relation to the sample thermocouple data.

Shown in figure 25 is a correlation of windward-side heating data obtained in both flight and wind-tunnel tests. The data are presented in terms of the Stanton number as a function of the local Reynolds number. The values for N_{St}^* and $N_{Re,x}^*$ are based on the assumption of isentropic stream-tube flow from the stagnation region and properties evaluated at Eckert's reference enthalpy. The reference length used in the $N_{Re,x}^*$ was the surface distance from the heat-shield stagnation point. The lines represent the theoretical level of heating to a flat plate at $\alpha = 0^\circ$ for the condition indicated. Data obtained on the forward portion of the cabin (S/R = 1.59) are best represented in the range of comparison by the laminar-attached theory until a critical Reynolds number is reached. Data obtained further aft on the cabin (S/R = 2.50) initially tend to follow the laminar-separated theory, and then the laminar-attached theory until a critical Reynolds number is attained. Beyond the critical Reynolds number, the Stanton numbers for both points on the cabin increase rapidly and approach turbulent values. The level of heating on the RCS section S/R = 3.12 is somewhat above the flat-plate value, but the data exhibit the laminar trend until transition occurs at approximately $N_{Re,x}^* = 1.5 \times 10^5$. The agreement of data from the three flights in terms of N_{St}^* and $N_{Re,x}^*$ at a given location is very good in most cases.

An attempt to correlate heat-transfer data obtained over the leeward side of the Gemini II spacecraft during reentry in terms of N_{St}^* and $N_{Re,x}^*$ is shown in figure 26. The lines labeled laminar-attached and laminar-separated were obtained as just described, and are shown here for comparative purposes. The discrepancy between the data and theoretical curves increases with increasing $N_{Re,x}^*$ until transitional values are attained. The third line shown in the figure has a slope of minus three-fourths which may be justified in the following manner. It has been shown (ref. 19) that for wedges and cones the ratio of base heating to attached heating just forward of separation varies inversely as the one-fourth power of Reynolds number. Because the attached heating value varies inversely as the one-half power, this yields a net dependence of base heating on $N_{Re,x}^{*-3/4}$. The laminar data are, in general, well correlated by a line with a minus three-fourths dependence on $N_{Re,x}^*$. This result was also obtained for separated flow regions on the Mercury spacecraft. The transition Reynolds number, which is taken to be the point at which the slope of the experimental data departs from the minus three-fourths value, is approximately $N_{Re,x}^* = 2 \times 10^4$.

The local Reynolds number (based on isentropic stream-tube properties at the edge of the boundary layer and the surface distance from the stagnation point) at several locations on the Gemini II spacecraft during reentry is shown in figure 27 as a function of altitude. Transition points have been determined from figures 25 and 26 (or similar plots for points not shown), and are tabulated in figure 27. The Gemini II spacecraft transition points in terms of the local Reynolds numbers are indicated on the curves by circular symbols. A comparison of the transition points indicates that transition occurred in at least three stages on the afterbody of the Gemini II spacecraft.

The separated flow region over the leeward side of the vehicle was the first to undergo transition. Data for the rearward portion of the cabin (S/R = 2. 50) and the RCS (S/R = 3. 12) indicate that transition occurred at those points at an altitude of 189 000 feet. At very nearly the same time, transition occurred over the forward portion of the cabin leeward side (S/R = 1. 83). At an altitude of about 160 000 feet, transition occurred on the windward side of the RCS. Laminar heating continued over the windward side of the cabin section for about 20 seconds, after which the entire afterbody was subjected to transitional or turbulent heating. Data for the Mercury spacecraft (ref. 7) are given in figure 27 for comparative purposes. It is shown that flow over the aft portion of the cabin and the cylindrical section of the Mercury spacecraft underwent transition at the same altitude as did the flow over similar areas of the leeward side of the Gemini spacecraft. Flow over the forward portion of the Mercury cabin remained laminar for a short while longer, and underwent transition at the same Reynolds number as did flow over the forward portion of the leeward side of the Gemini cabin. Thus, it is shown that the separated flow over the leeward side of the Gemini spacecraft undergoes transition at conditions similar to those for which transition occurred over the Mercury spacecraft. This tends to substantiate the contention (ref. 7) that the low values of transition Reynolds number obtained on the MA-5 spacecraft were attributable to the separated flow afterbody condition. The factor of 5 to 10 between the Gemini windward and leeward transition Reynolds numbers clearly indicates this to be the case as it is reasonably well established that the windward flow is attached while the leeward flow is separated.

CONCLUDING REMARKS

Heat-transfer and surface-pressure data over the afterbody of the Gemini spacecraft obtained during launch and reentry and also during wind-tunnel tests have been presented. These data have been interpreted in terms of nondimensionalized pressure distribution, aerodynamic heating rates, and Stanton numbers. The following data have been observed:

1. Wind-tunnel tests of the launch configuration yielded pressure data which were in good agreement with the flight data.

2. Heat-transfer data from both wind-tunnel and flight tests, presented in terms of Stanton numbers, are in satisfactory agreement with each other and with theory. These data also show that flow over the entire spacecraft during launch is turbulent or transitional when highest heating rates occur.

3. The initial afterbody heating during reentry may be characterized as caused by either laminar-attached or laminar-separated flow, depending on the location; but after transition to turbulent flow occurs, the heating over the entire windward side arises from a turbulent-attached flow.

4. Windward-side heat-transfer data presented in terms of Stanton numbers are in reasonable agreement with the wind-tunnel data and with flat-plate theories.

5. Transition to turbulent flow over the spacecraft during reentry occurred in three stages: transition over the entire leeward side occurred first, followed by transition over the windward side of the reentry control system and the rendezvous and recovery section. Transition over the windward side of the cabin occurred approximately 20 seconds after transition on the rendezvous and recovery section and the reentry control system.

6. Heating rates over the leeward side of the rendezvous and recovery section were found to exceed the windward side values for certain angle-of-attack conditions.

7. Laminar heat-transfer rates over the leeward side of the spacecraft show a minus three-fourths dependence on Reynolds number based on surface distance from the stagnation point and local conditions evaluated at the reference enthalpy rather than the minus one-half variation typical of laminar flow on flat plates.

Manned Spacecraft Center
National Aeronautics and Space Administration
Houston, Texas, March 1, 1967
923-50-89-00-72

REFERENCES

1. Everhart, Philip E.; and Bernot, Peter T.: Measurements of the Surface Flows, Heat Transfer, Pressure Distribution, and Longitudinal Stability of a Mercury Capsule Model at Mach Numbers of 6.9 and 9.6. NASA TM X-458, 1961.

2. Newlander, Robert A.; Taylor, Nancy L.; and Pritchard, E. Brian: Pressure Distribution on Two Models of a Project Mercury Capsule for a Mach Number Range of 1.60 to 6.01 and an Angle-of-Attack Range of 0° to 180°. NASA TM X-336, 1960.

3. Reller, John O., Jr.; and Seegmiller, H. Lee: Pressure and Heat-Transfer Measurements on a Mercury Capsule Model. NASA TM X-647, 1962.

4. Taylor, Nancy L.; Hodge, Ward F.; and Burbank, Paige B.: Heat-Transfer and Pressure Measurements of a 1/7-Scale Model of a Mercury Capsule at Angles of Attack from 0° to +20° at Mach Numbers of 3.50 and 4.44. NASA TM X-522, 1961.

5. Weston, Kenneth C.; and Swanson, Joanna E.: A Compilation of Wind-Tunnel Heat-Transfer Measurements on the Afterbody of the Project Mercury Capsule Reentry Configuration. NASA TM X-495, 1961.

6. Stephens, Emily W.: Afterbody Heating Data Obtained From an Atlas-Boosted Mercury Configuration in a Free Body Reentry. NASA TM X-493, 1961.

7. Weston, Kenneth C.; and Fitzkee, Archie L.: Afterbody Heat Transfer Measurements Obtained During Reentry of the Spacecraft of the Mercury-Atlas 5 Mission. NASA TM X-564, 1963.

8. Murphy, J. D.: Flight Test Aerodynamics Heating Data for the Afterbody of the Project Mercury Spacecraft with Comparison to Available Prediction Methods. NASA CR-649, 1967.

9. Price, Earl A.; Stallings, Robert C.; and Howard, Paul W.: Pressure and Heat-Transfer Distributions of 0.1-Scale Gemini Exit and Reentry Models at Mach Numbers of 3.51 and 4.44. NASA TM X-1149, 1965.

10. Miguel, J. J.: Hypersonic Wind Tunnel Pressure and Heat Transfer Tests of 10 Percent Gemini Models at the Arnold Engineering Development Center. Rept. 9407, McDonnell Aircraft Corp., Jan. 1965.

11. Harrington, S. A.: Hypersonic Pressure and Heat-Transfer Tests of the Gemini Reentry Capsule for McDonnell Aircraft Corporation. Rept. No. AA-1711-Y-1, Cornell Aeronautical Laboratory, Nov. 1962.

12. Anon.: Manual for Users of the Unitary Plan Wind Tunnel Facilities of the National Advisory Committee for Aeronautics, 1956.

13. Anon.: Test Facilities Handbook. Fourth ed., Arnold Engineering Development Center, 1962.

14. Anon.: Cal 48" Hypersonic Shock Tunnel Description and Capabilities. Cornell Aeronautical Laboratory, 1962.

15. Stoney, William E., Jr.: Heat Transfer to Blunt Noses at High Supersonic Speeds. Paper presented at NACA Conference on Aircraft Loads, Structures, and Flutter. Langley Aeronautical Laboratory (Langley Field, Va.), Mar. 5 to 7, 1957.

16. Stine, Howard A.; and Wanlass, Kent: Theoretical and Experimental Investigation of Aerodynamic-Heating and Isothermal Heat-Transfer Parameters on a Hemispherical Nose with Laminar Boundary Layer at Supersonic Mach Numbers. NACA TN 3344, 1954.

17. Chapman, Dean R.: A Theoretical Analysis of Heat Transfer In Regions of Separated Flow. NASA TN D-3792, 1956.

18. Bertin, John J.: Wind-Tunnel Heating Rates for the Apollo Spacecraft. NASA TM X-1033, 1965.

19. Baum, E.; King, H. H.; and Denison, M. R.: Recent Studies of the Laminar Base Flow Region. Preprint 64-5, AIAA, Jan. 1964.

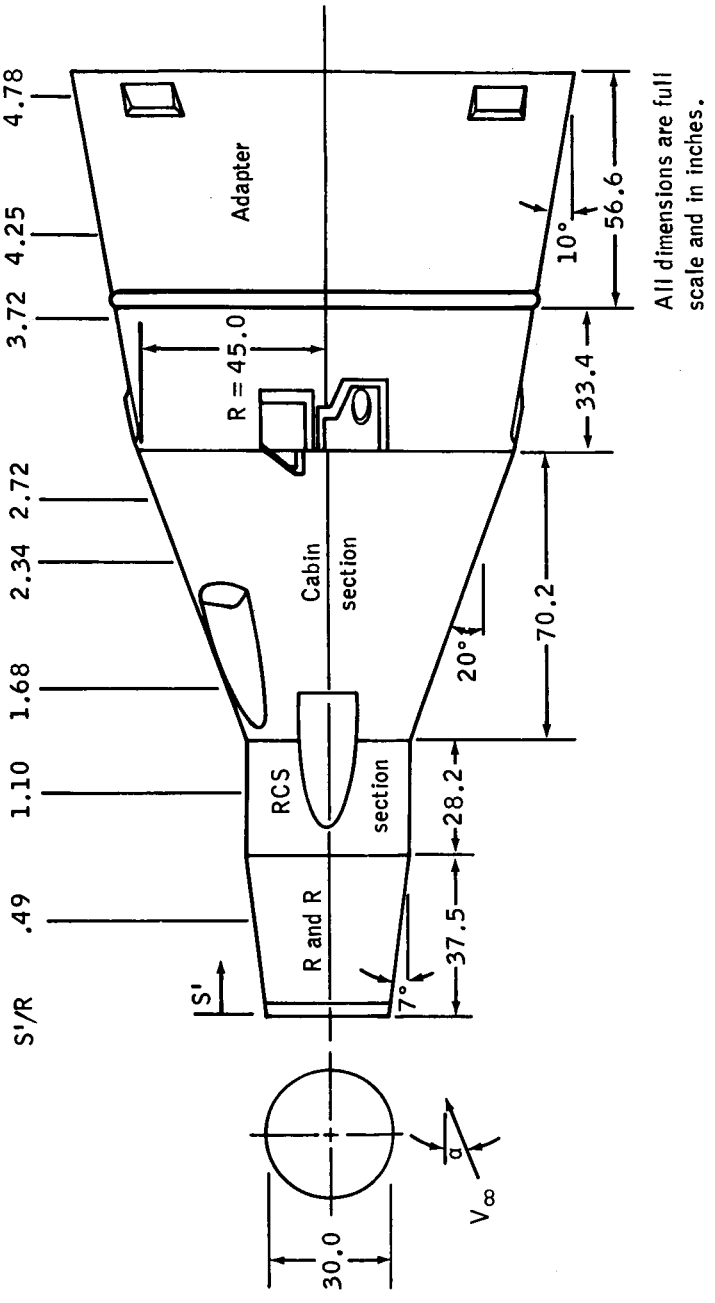

(a) Exit configuration.

Figure 1. - The Gemini spacecraft.

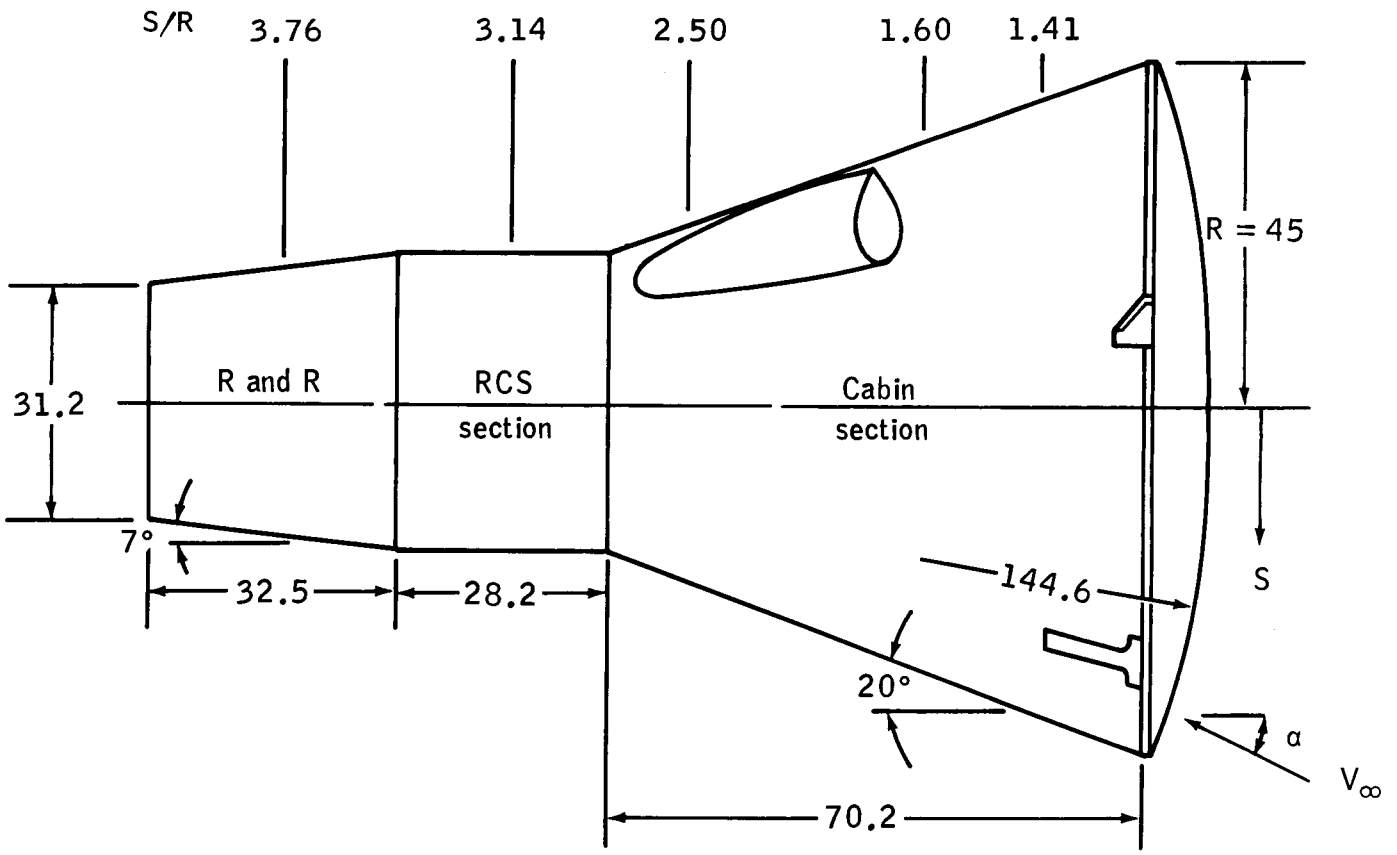

All dimensions are full scale and in inches.

(b) Reentry configuration.

Figure 1.- Concluded.

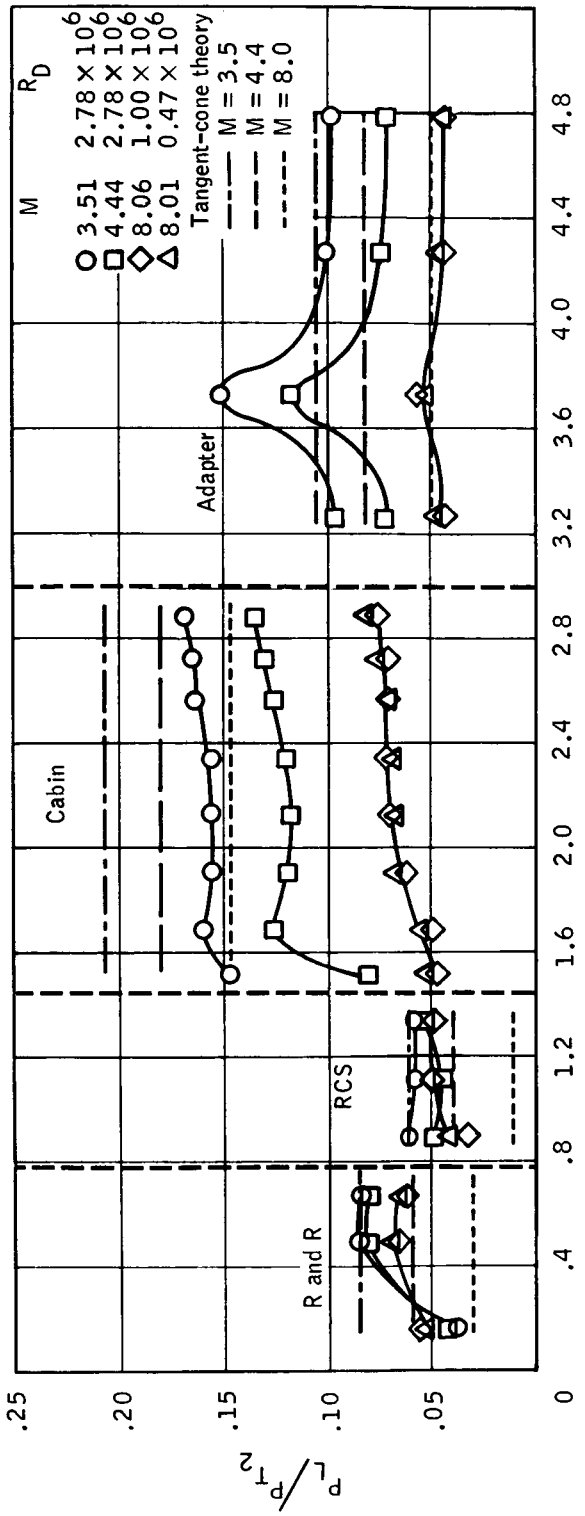

(a) $\alpha = 0°$.

Figure 2. - Exit configuration wind-tunnel pressure distribution.

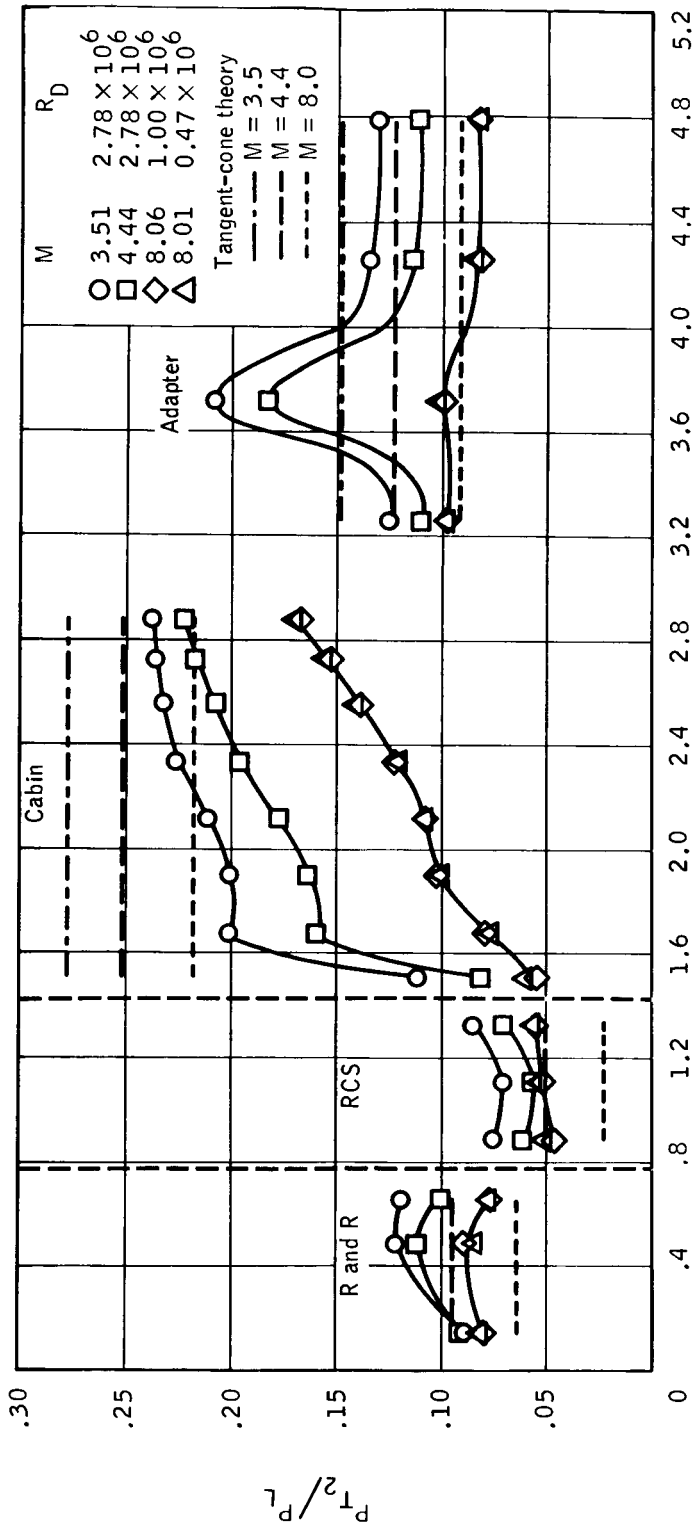

(b) $\alpha = 5^\circ$, windward side.

Figure 2.- Concluded.

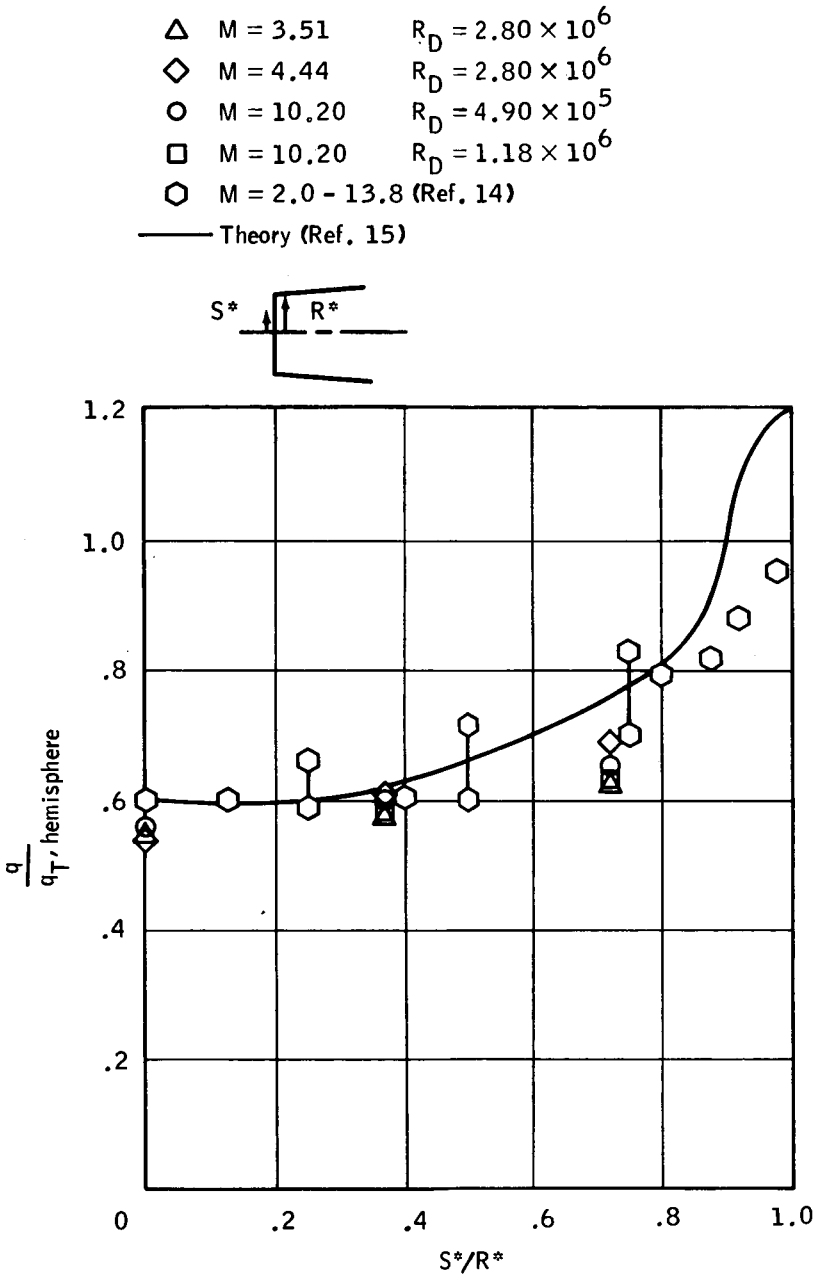

Figure 3. - Heating-rate distribution over the flat end of the R and R in the launch configuration.

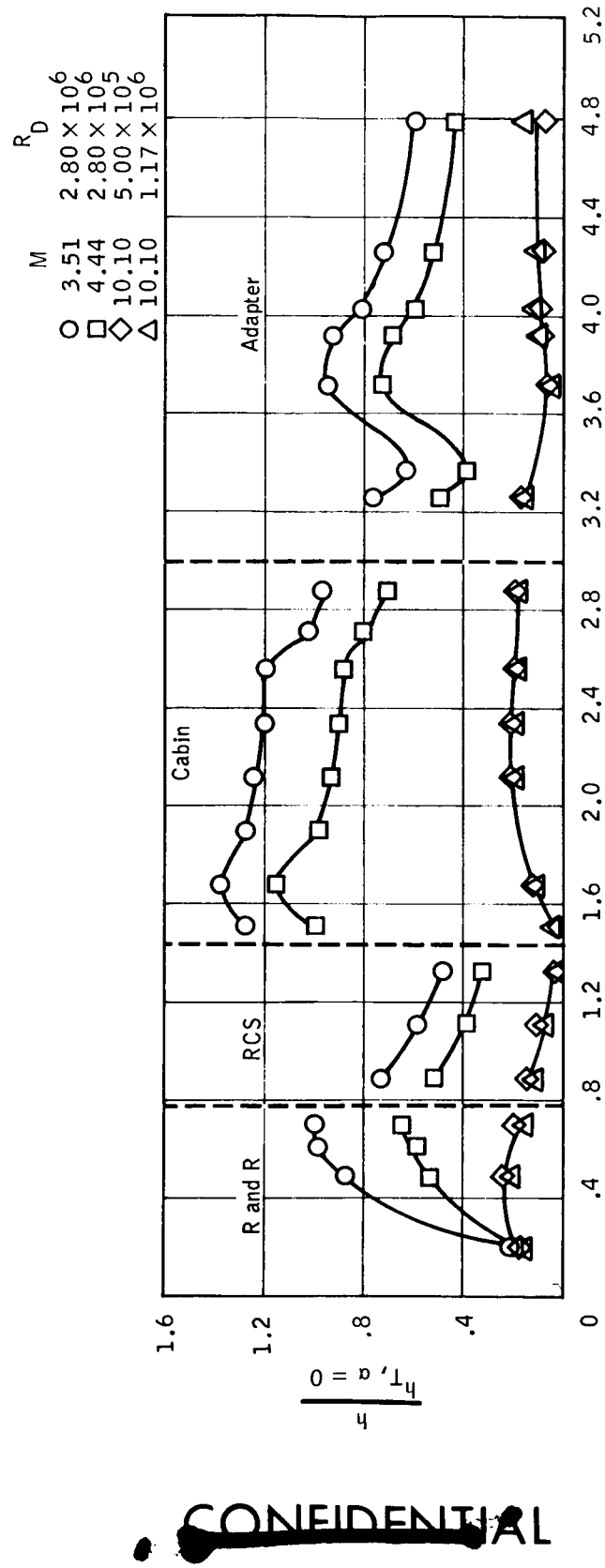

(a) $\alpha = 0°$.

Figure 4. - Exit configuration wind-tunnel heating distribution.

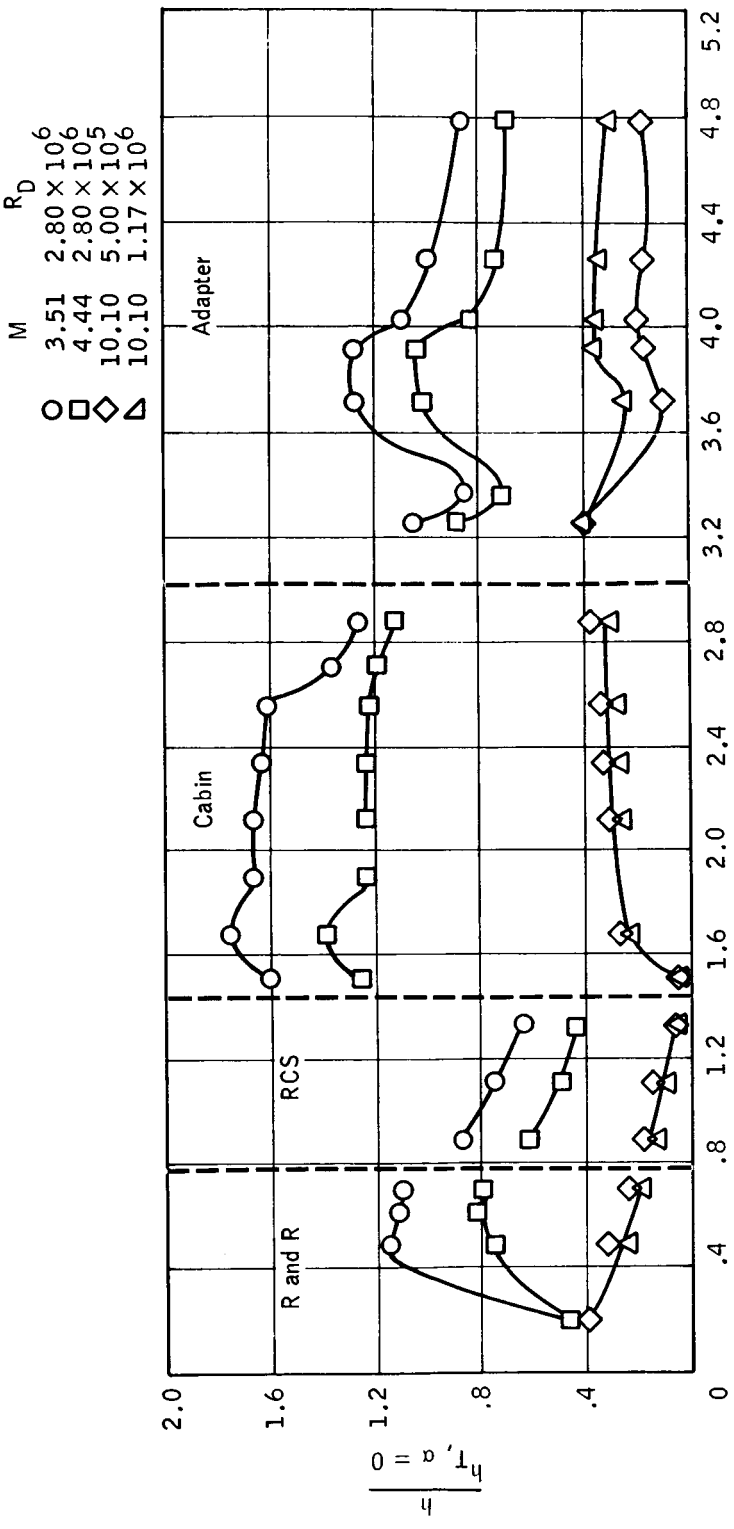

(b) $\alpha = 5^\circ$, windward side.

Figure 4. - Concluded.

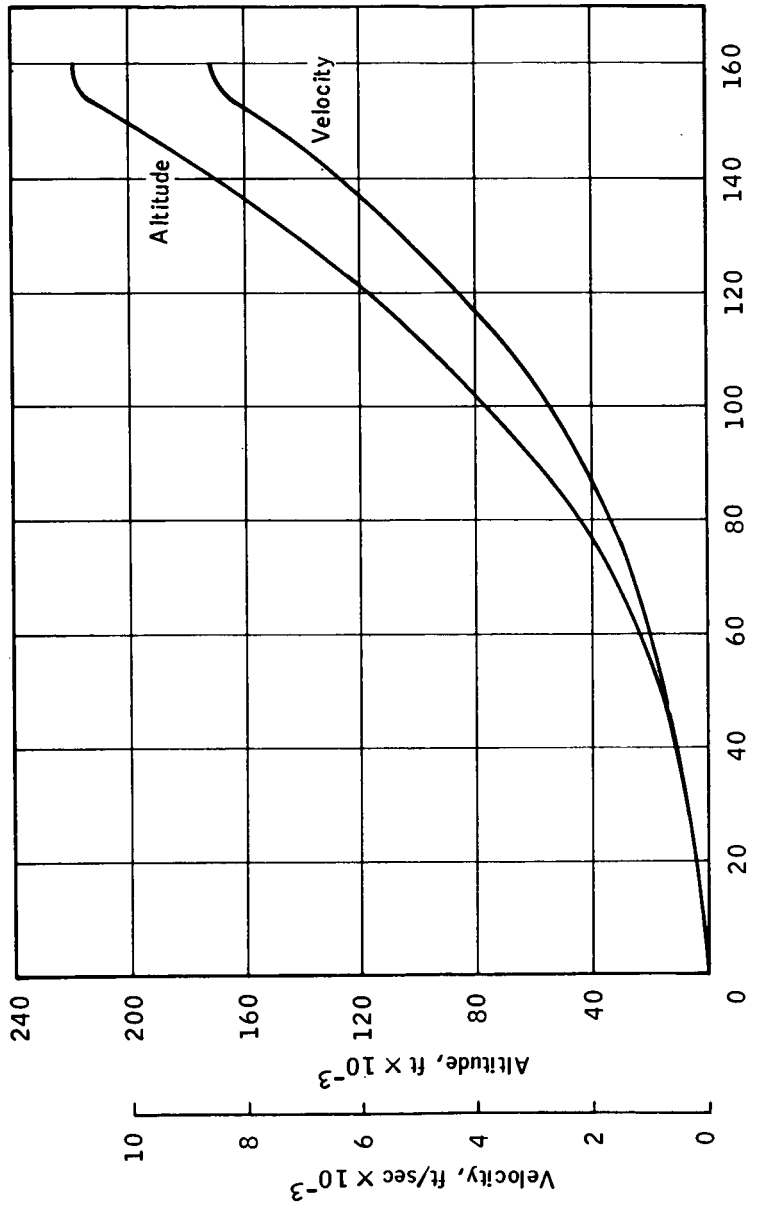

Figure 5. - Nominal Gemini launch trajectory.

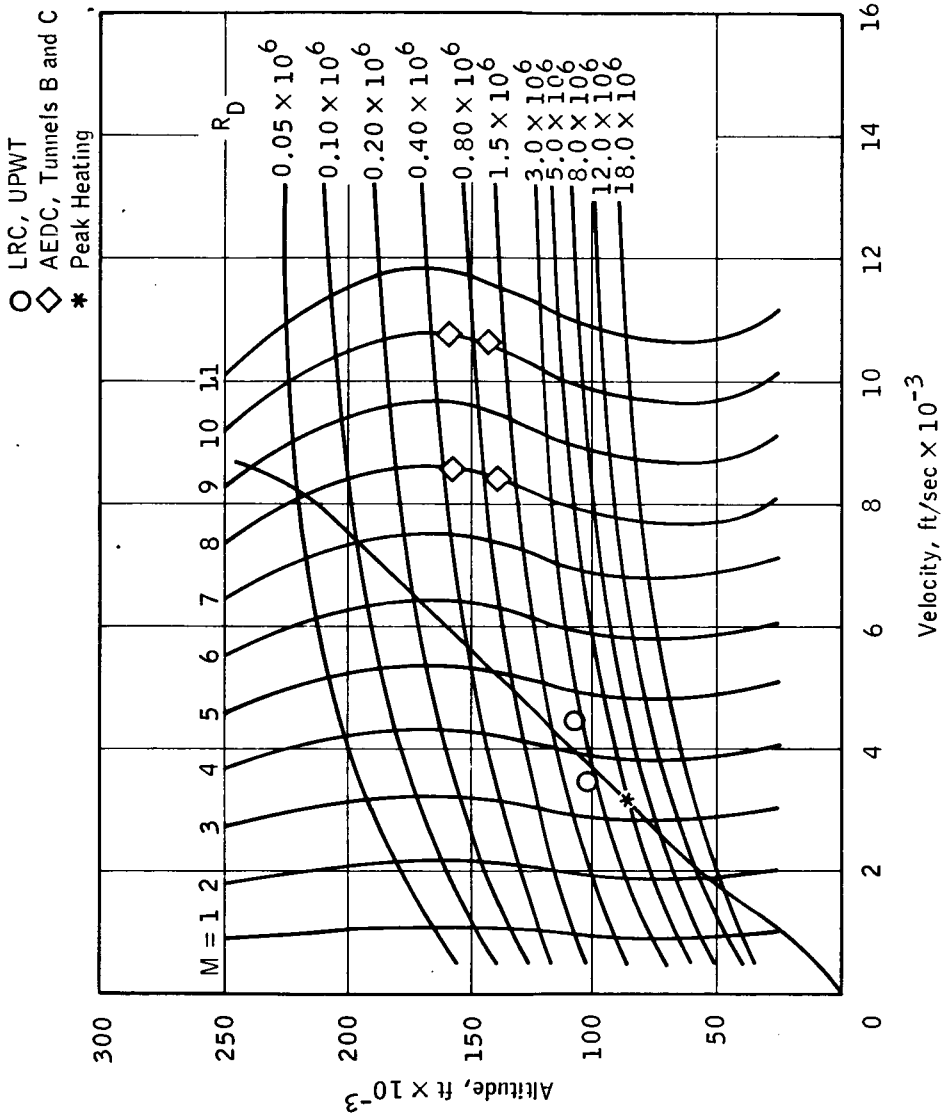

Figure 6. - Nominal Gemini launch aerodynamic environment, 1962 U.S. Standard Atmosphere.

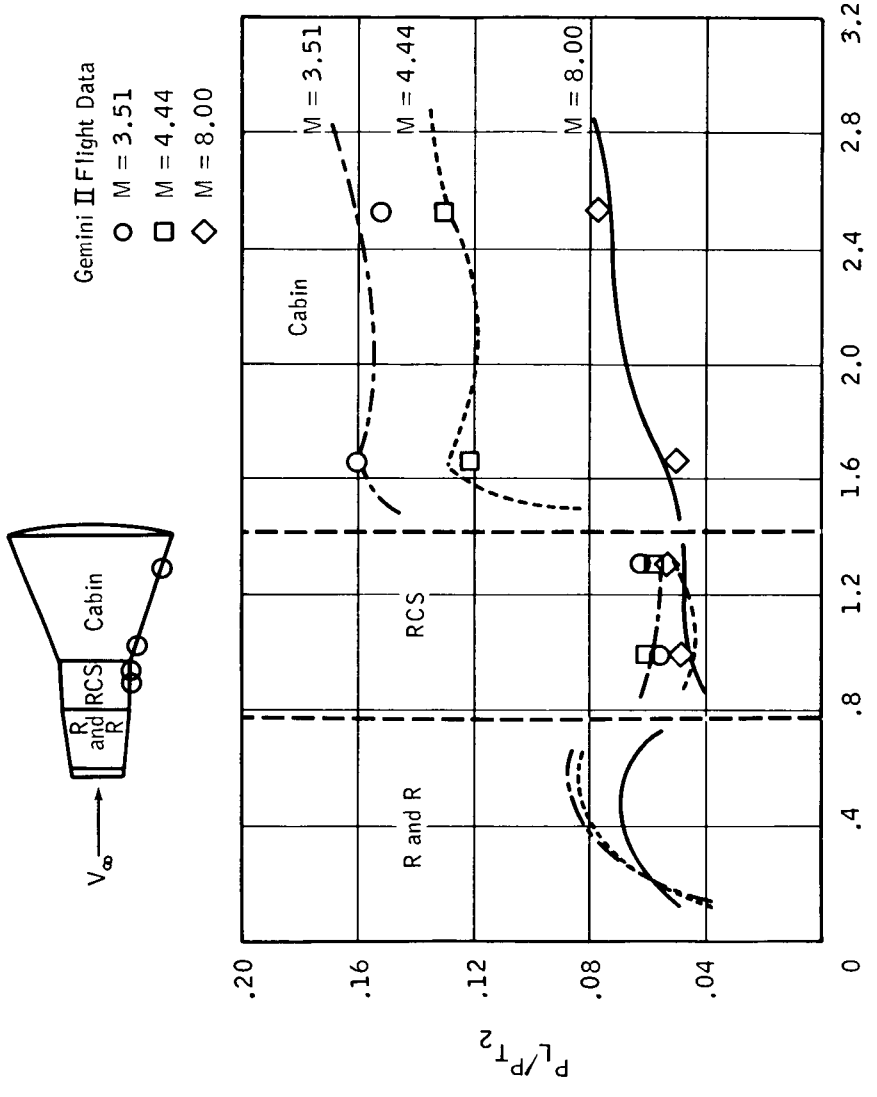

Figure 7. - Comparison of wind-tunnel and flight pressure distributions over the exit configuration.

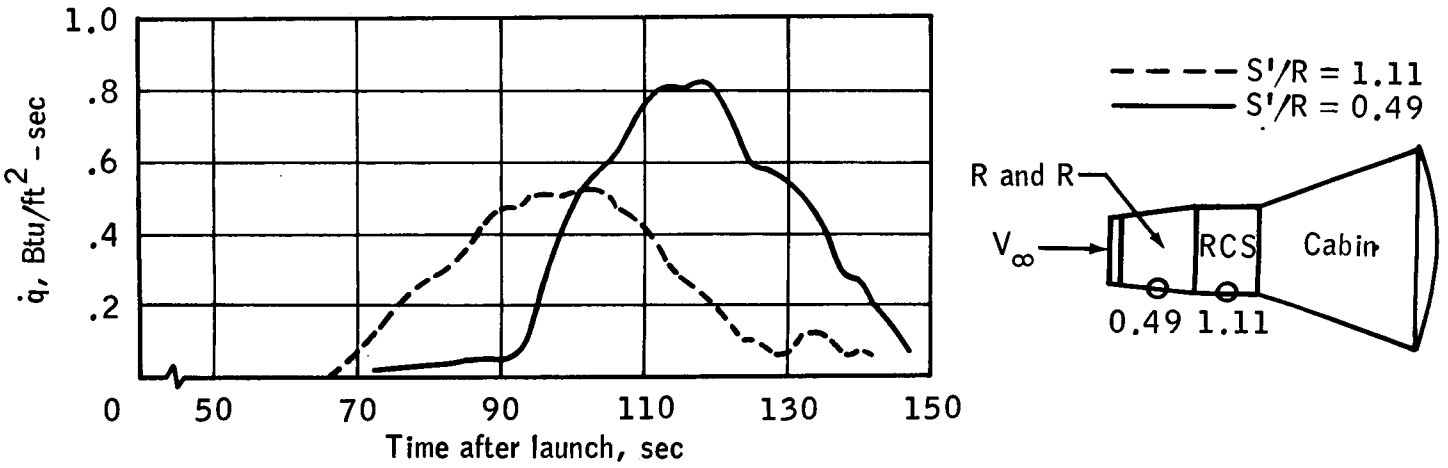

(a) RCS and R and R.

Figure 8. - Gemini II exit heating-rate histories.

CONFIDENTIAL

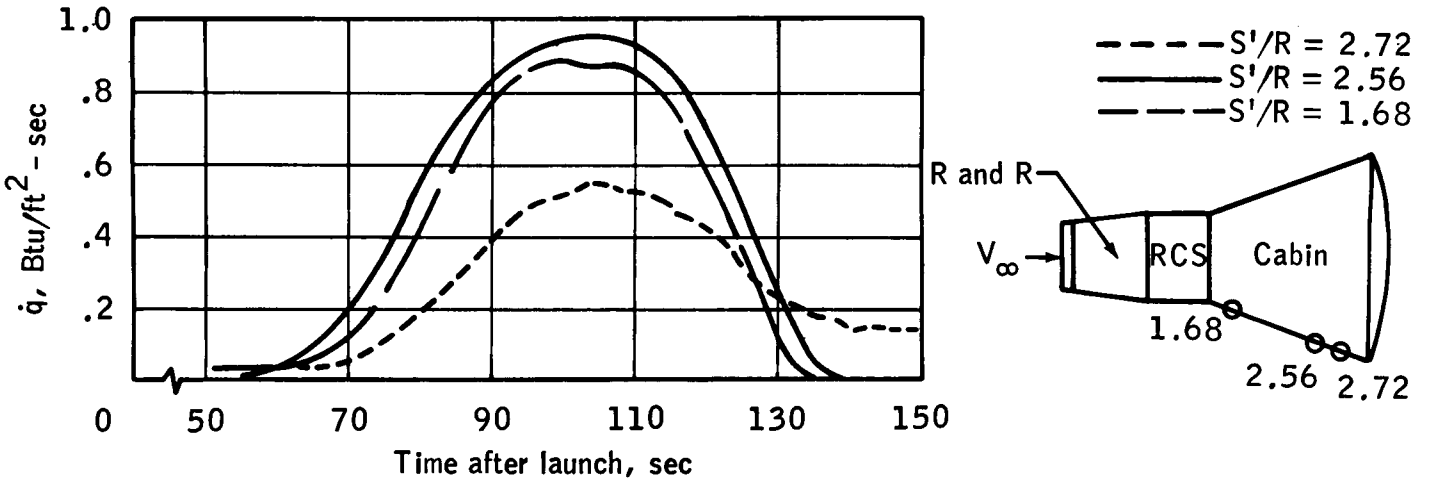

(b) Cabin.

Figure 8. - Concluded.

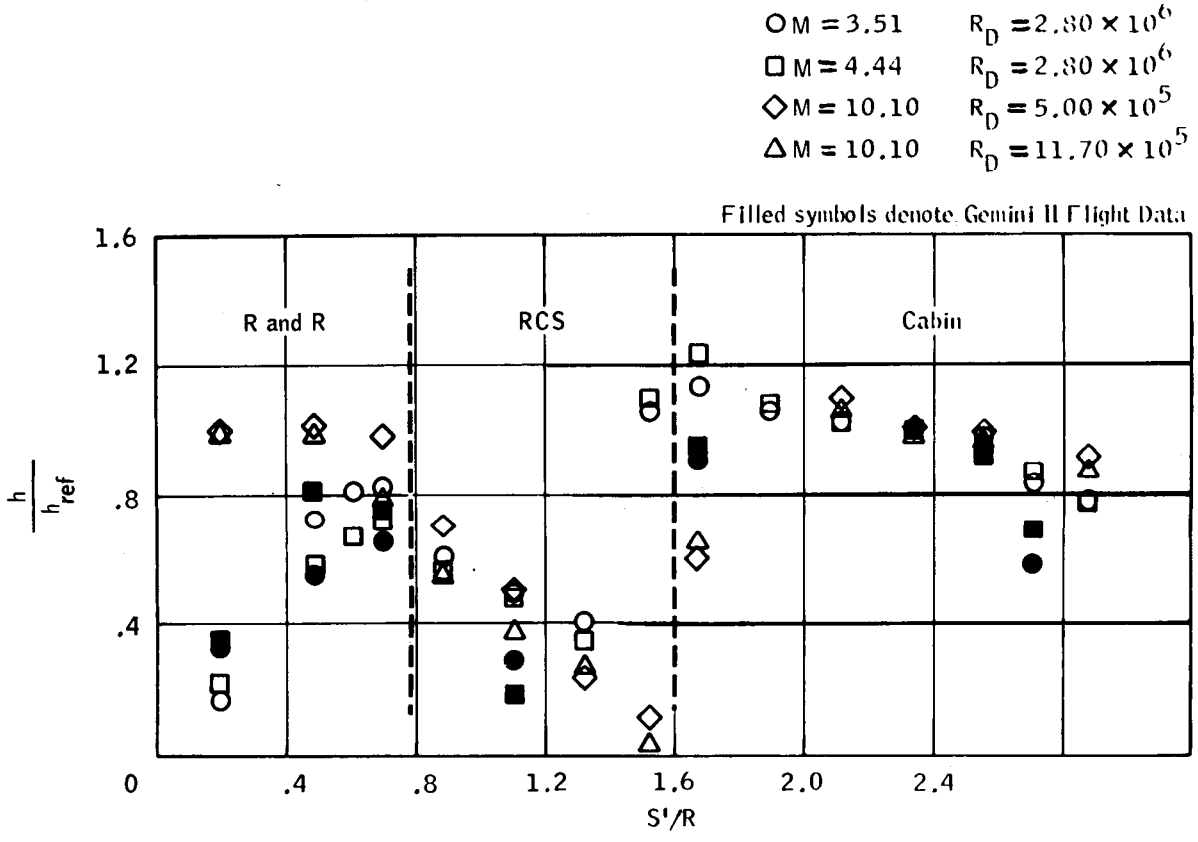

Figure 9. - Comparison of wind-tunnel and flight heat-transfer distributions over the launch configuration.

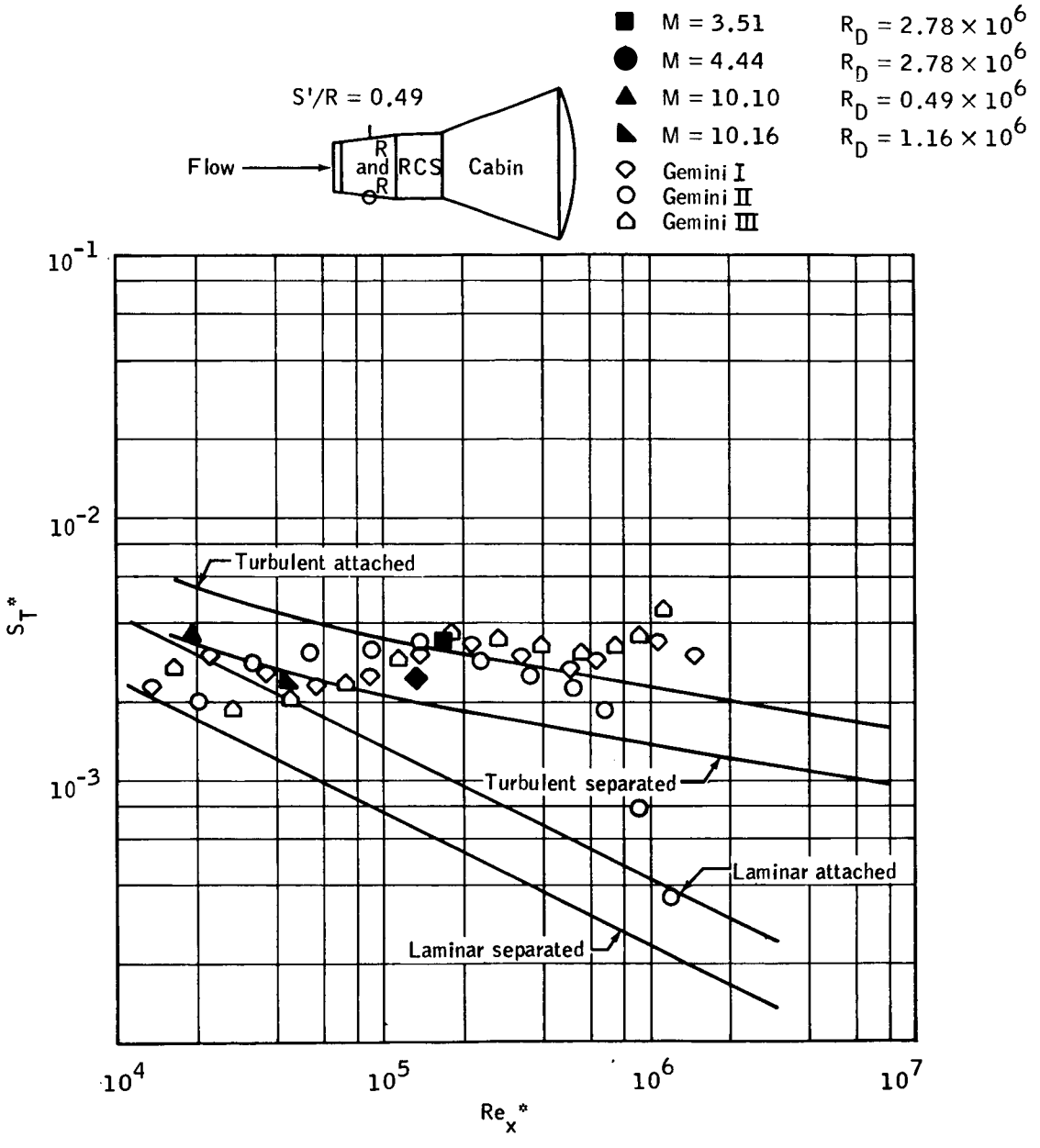

(a) S'/R = 0.49.

Figure 10. - Correlation of wind-tunnel and flight heat-transfer data.

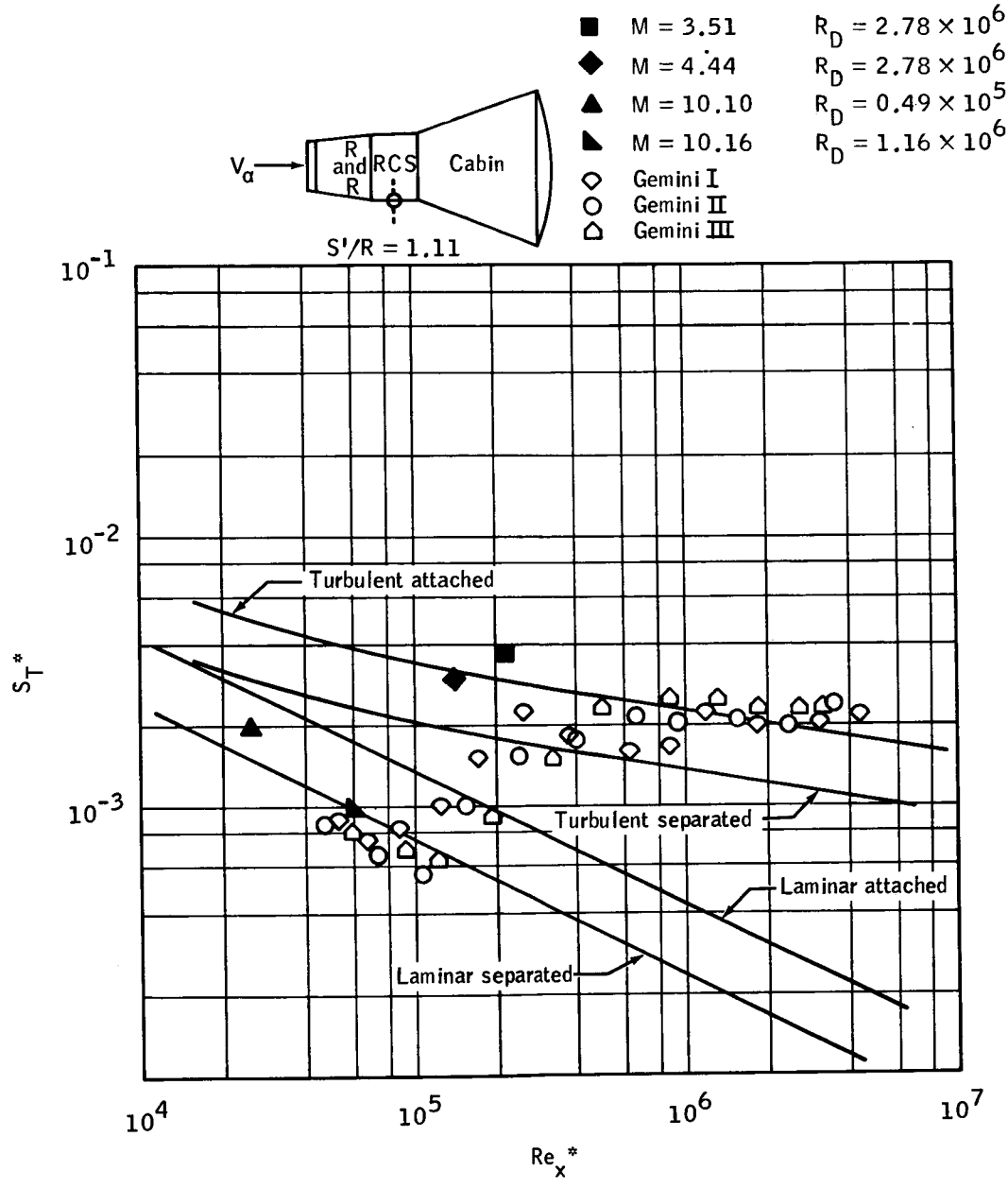

(b) S'/R = 1.11.

Figure 10. - Continued.

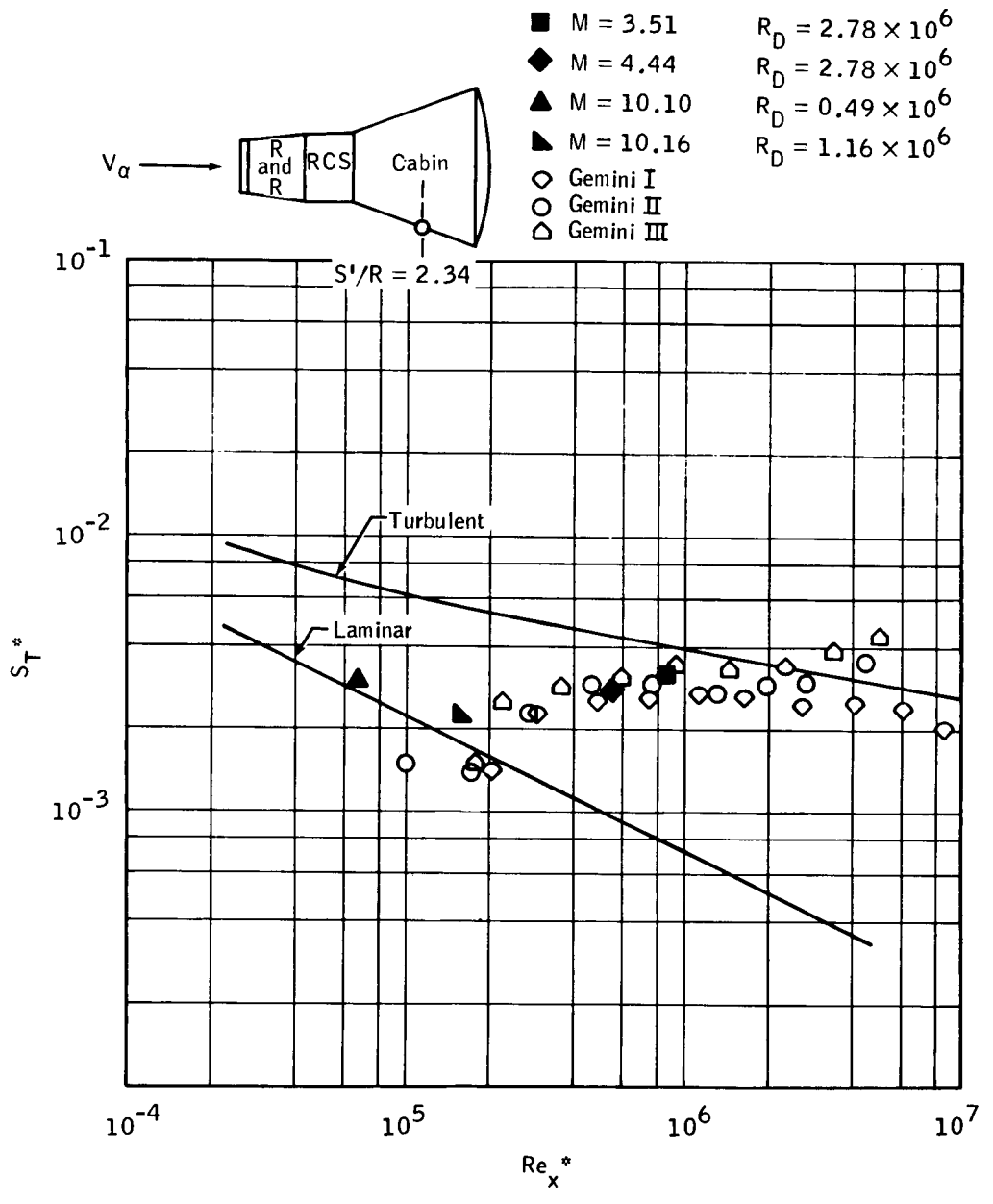

(c) S'/R = 2.34.

Figure 10. - Concluded.

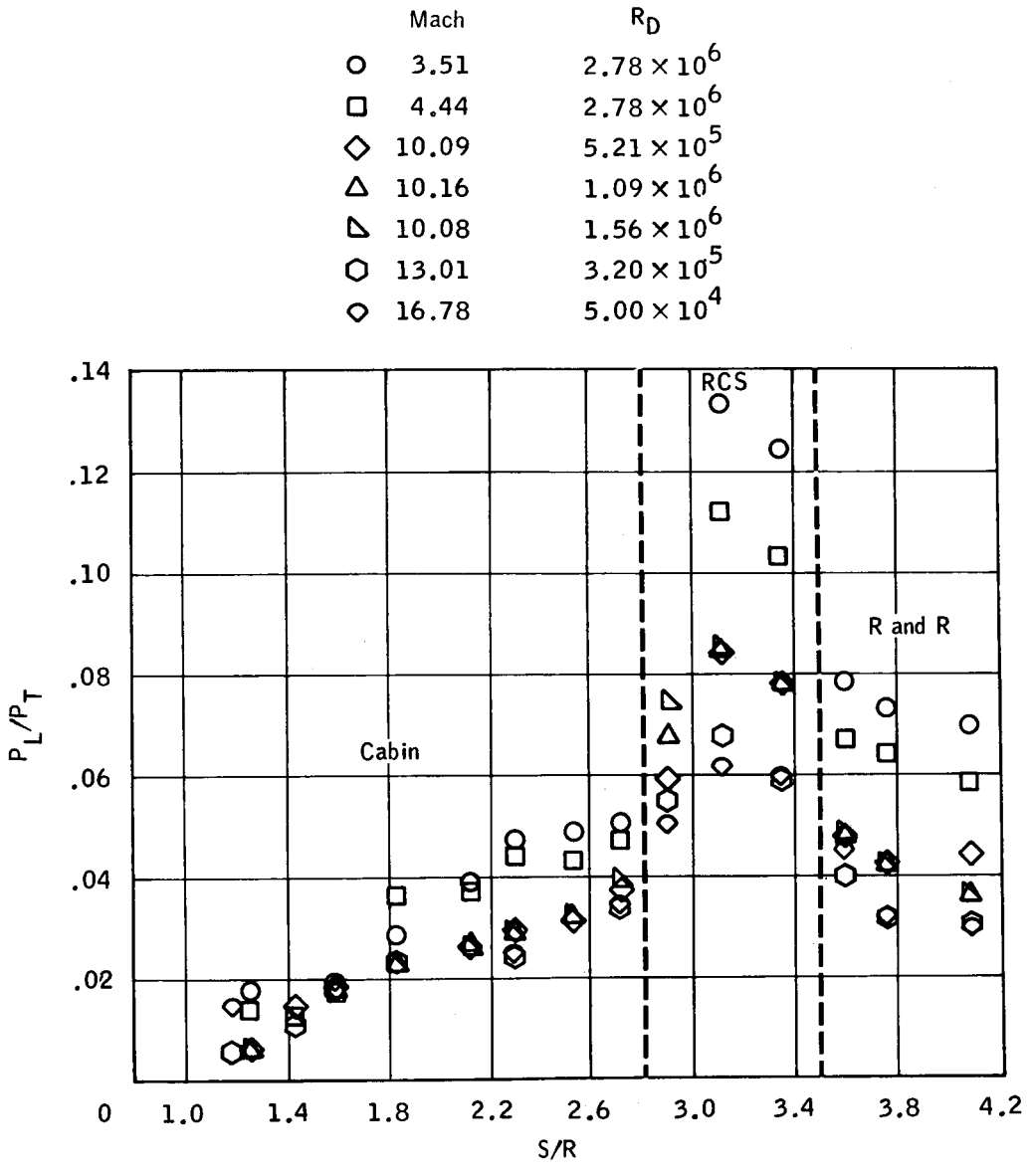

(a) $\alpha = 10°$.

Figure 11. - Wind-tunnel pressure distribution over the windward side of the reentry configuration afterbody.

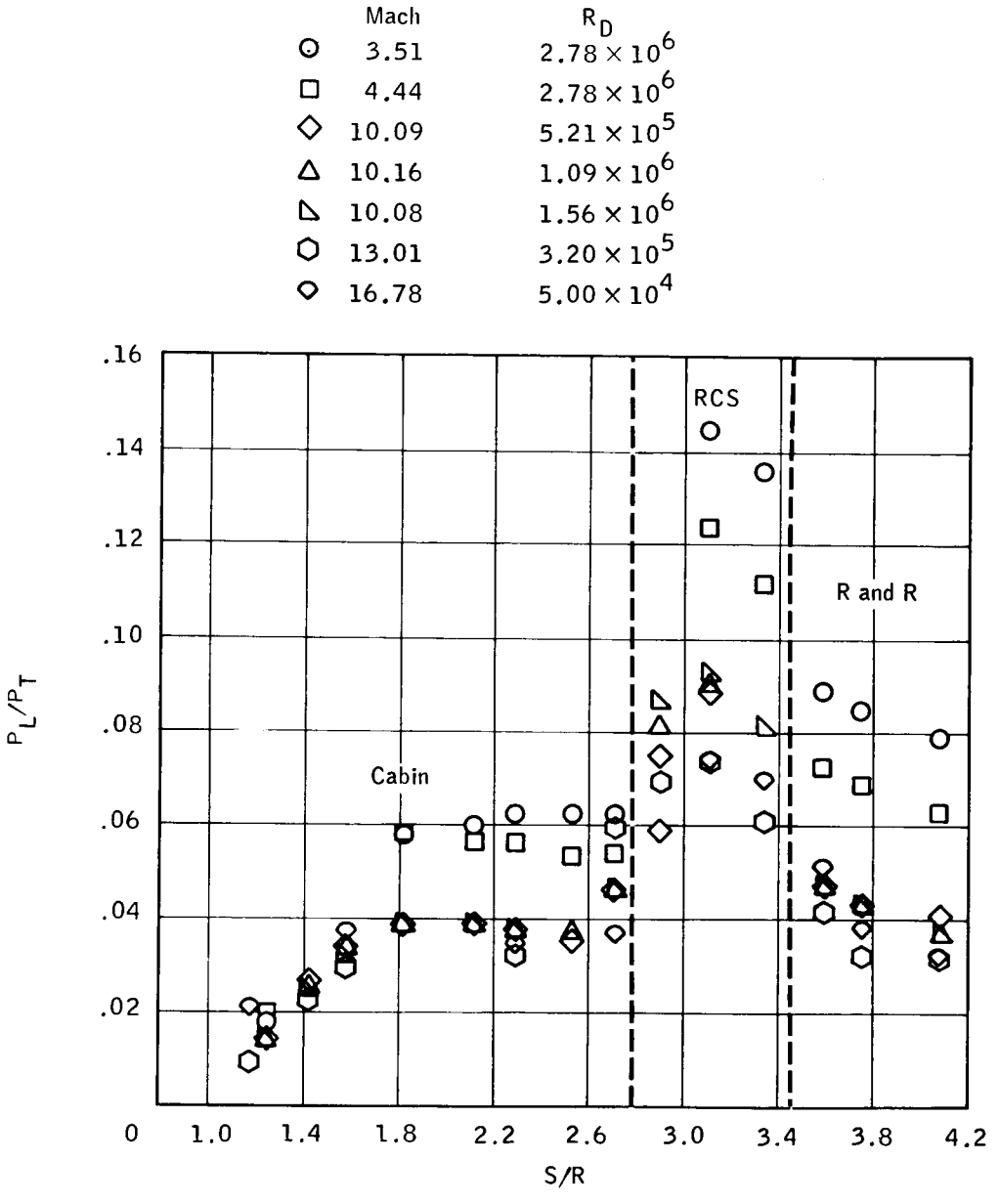

(b) $\alpha = 15°$.

Figure 11. - Continued.

	Mach	R_D
○	3.51	2.78×10^6
□	4.44	2.78×10^6
◇	10.09	5.21×10^5
△	10.16	1.09×10^6
◺	10.08	1.56×10^6
⬡	13.01	3.20×10^5
◇	16.78	5.00×10^4

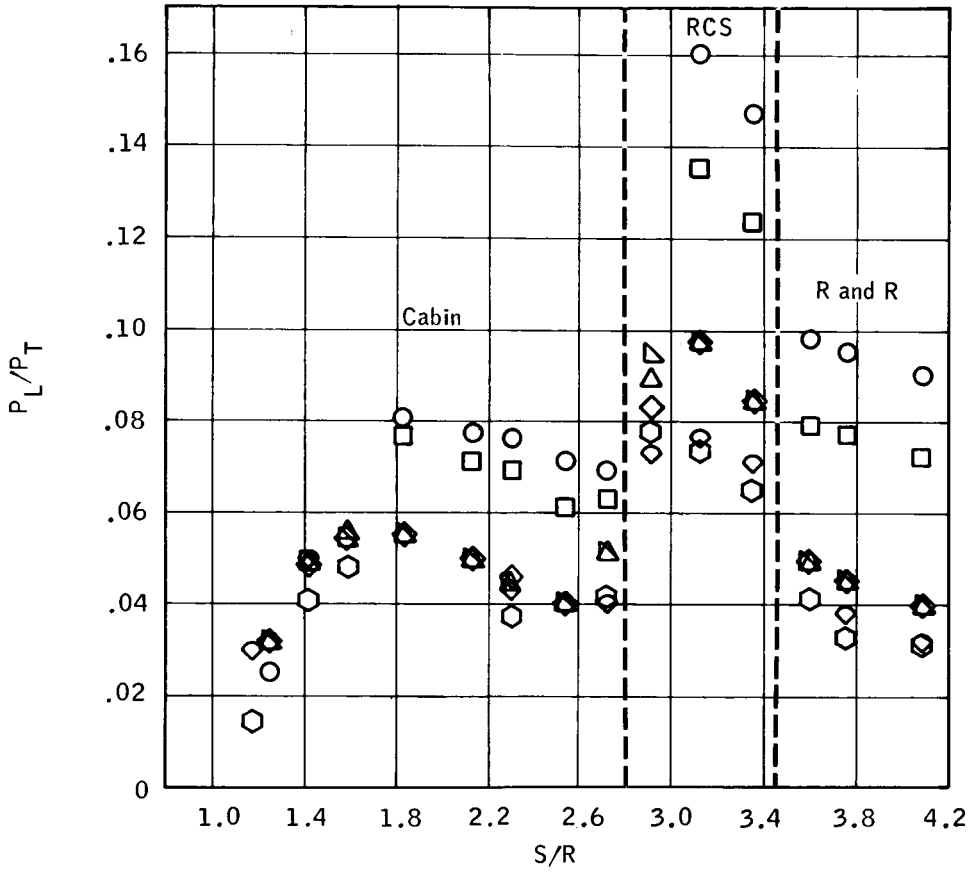

(c) $\alpha = 20°$.

Figure 11. - Concluded.

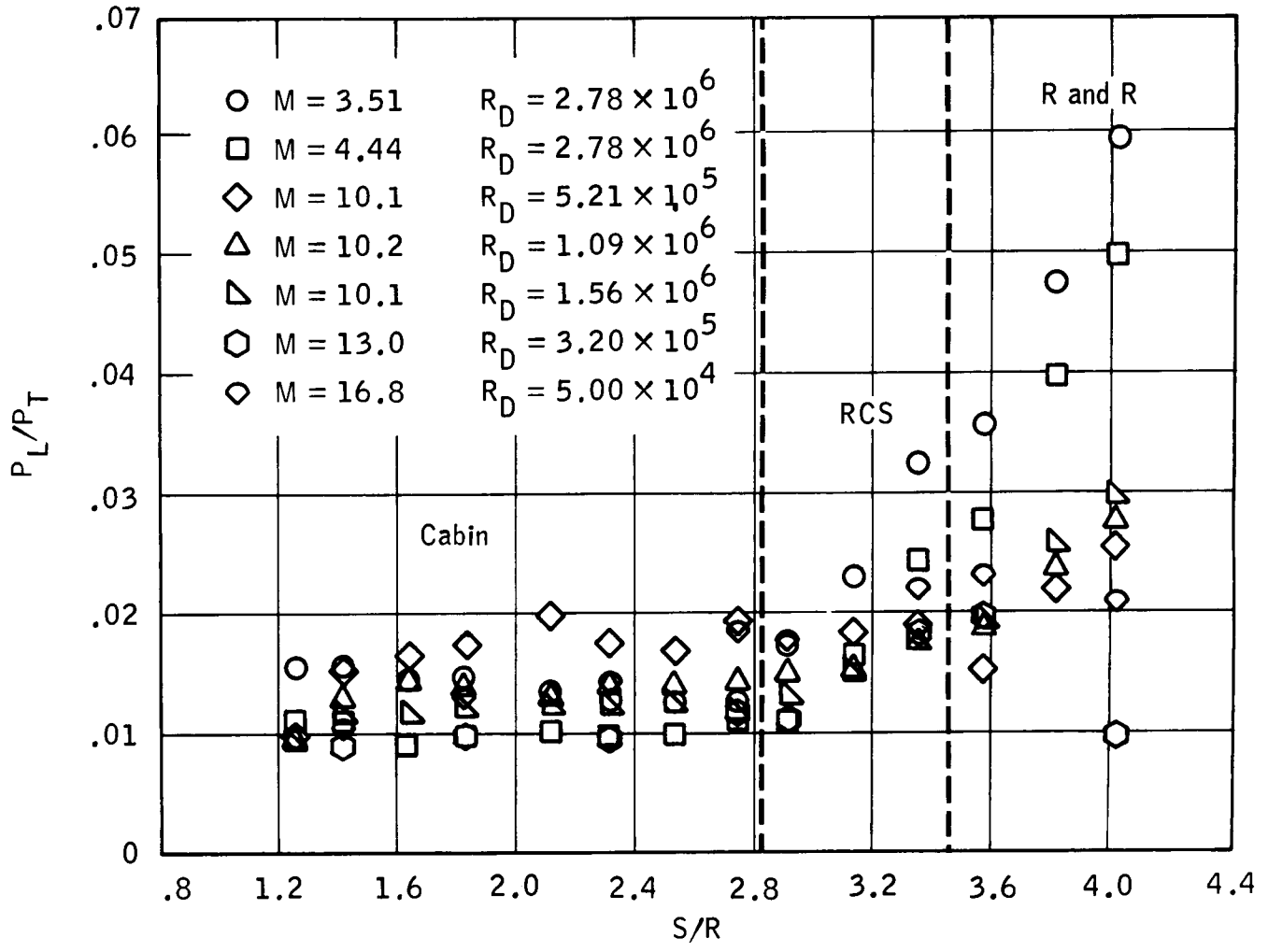

(a) $\alpha = 10°$.

Figure 12. - Wind-tunnel pressure distribution over the leeward side of the reentry configuration afterbody.

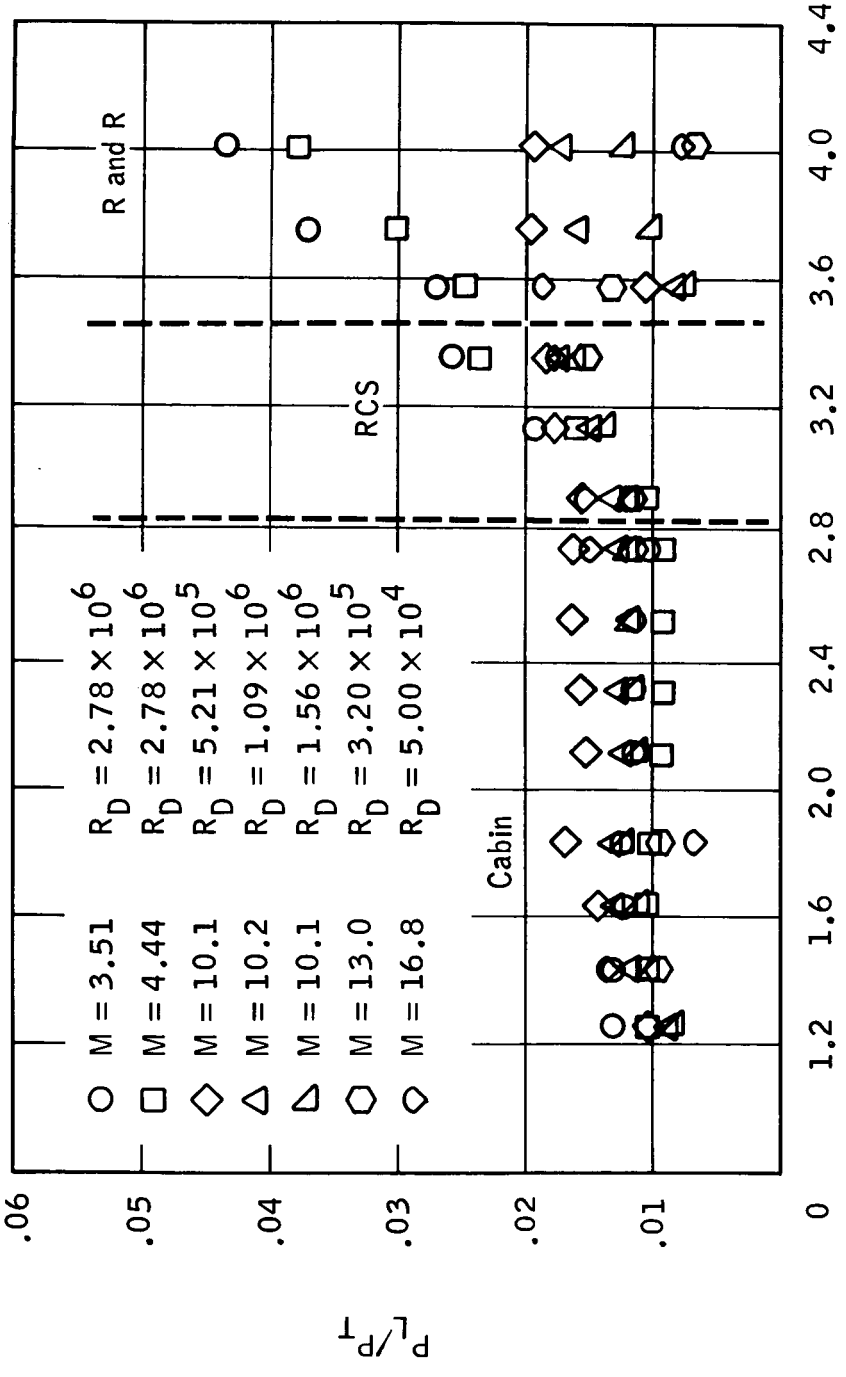

(b) $\alpha = 15°$.

Figure 12. - Continued.

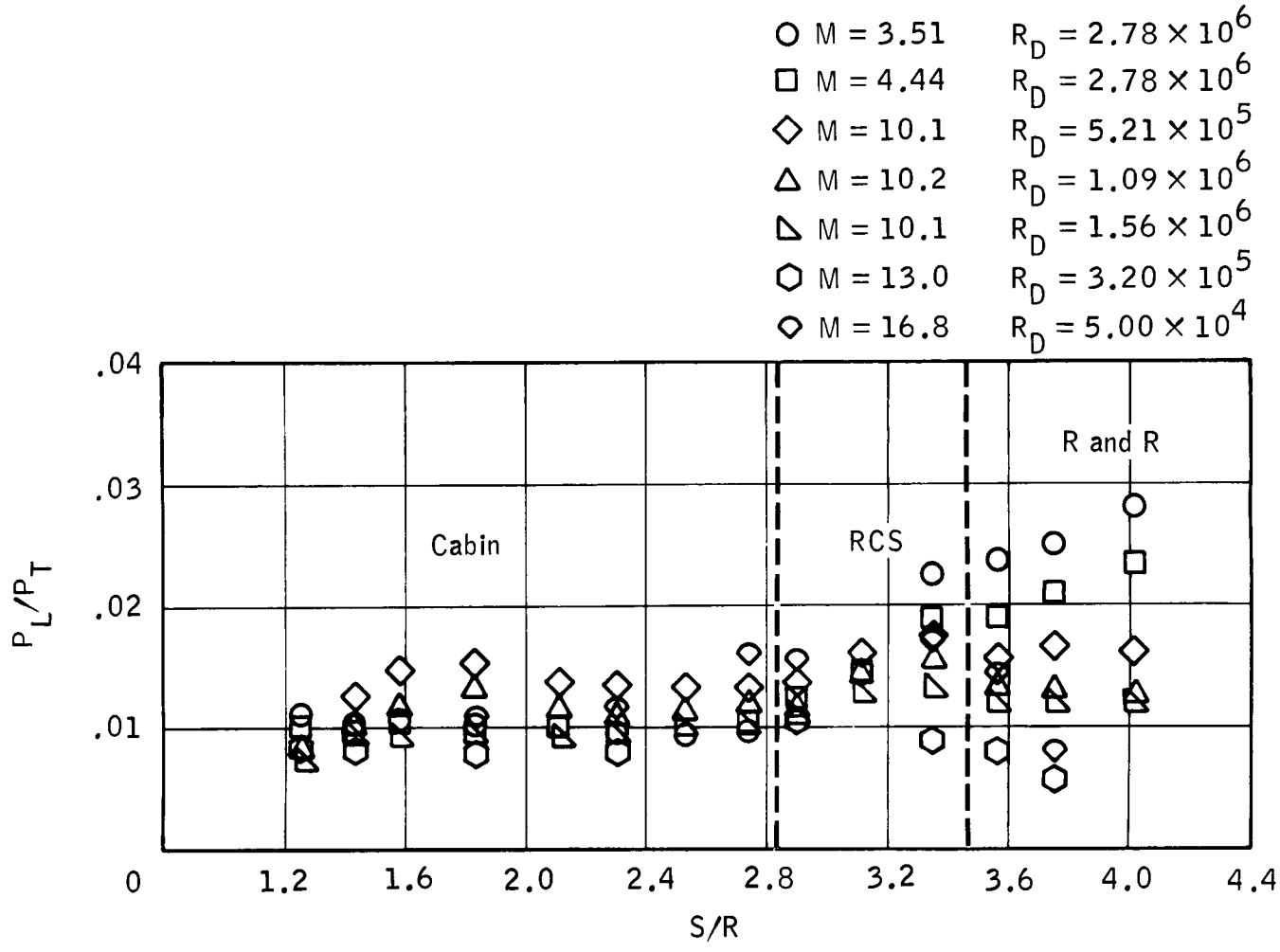

(c) $\alpha = 20°$.

Figure 12. - Concluded.

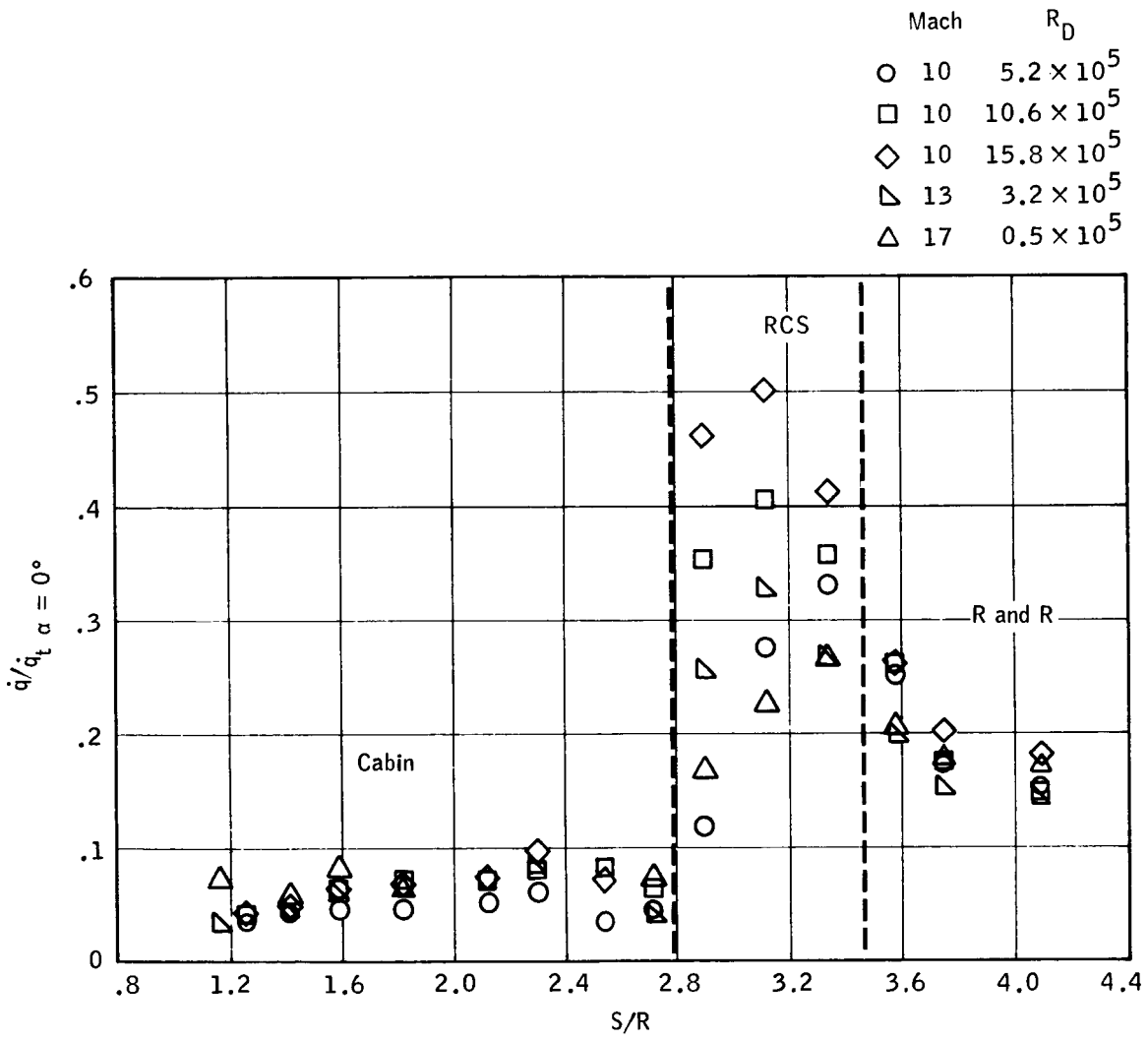

(a) $\alpha = 10°$.

Figure 13. - Wind-tunnel heat-transfer distribution over the windward side of the reentry configuration afterbody.

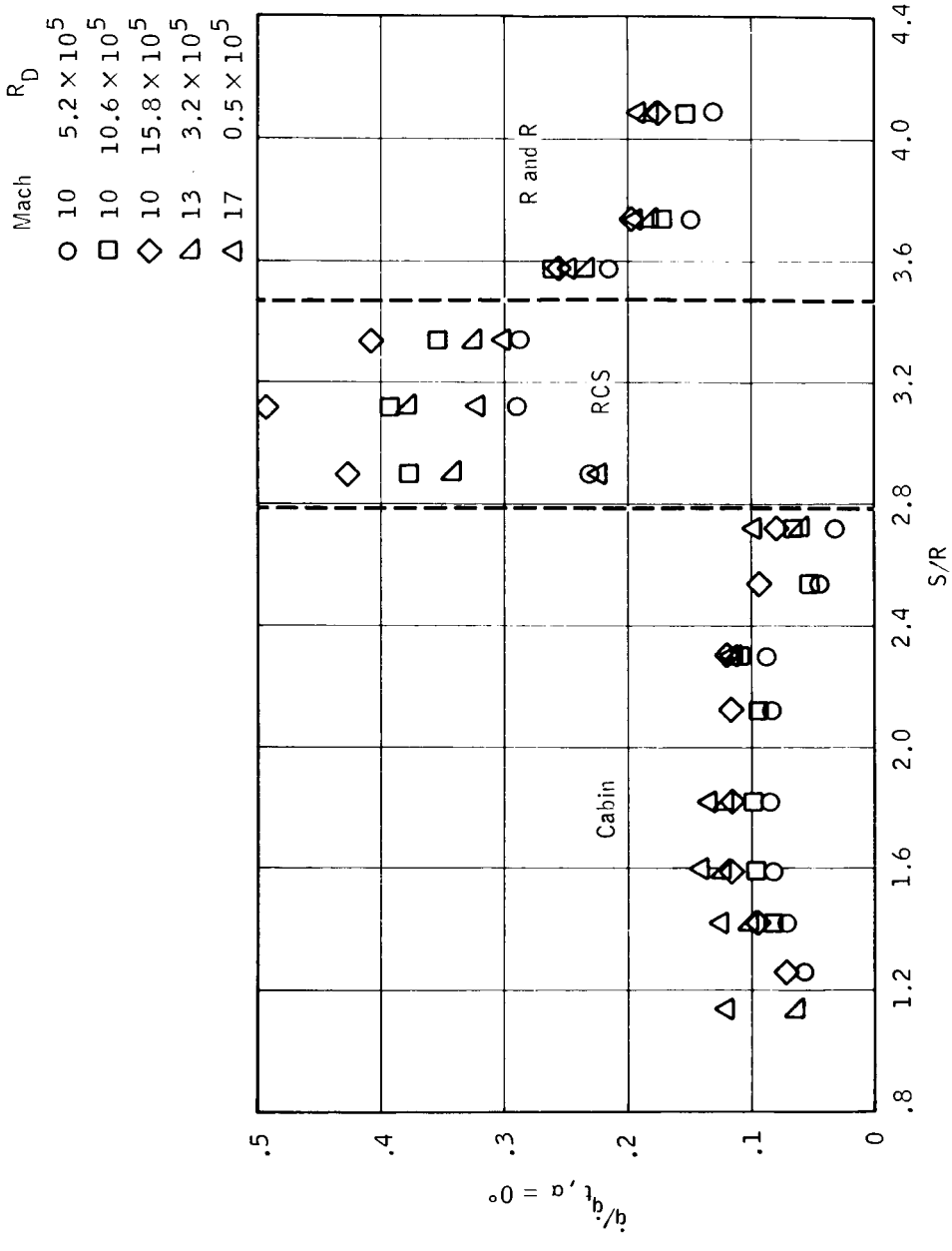

(b) $\alpha = 15°$.

Figure 13.- Continued.

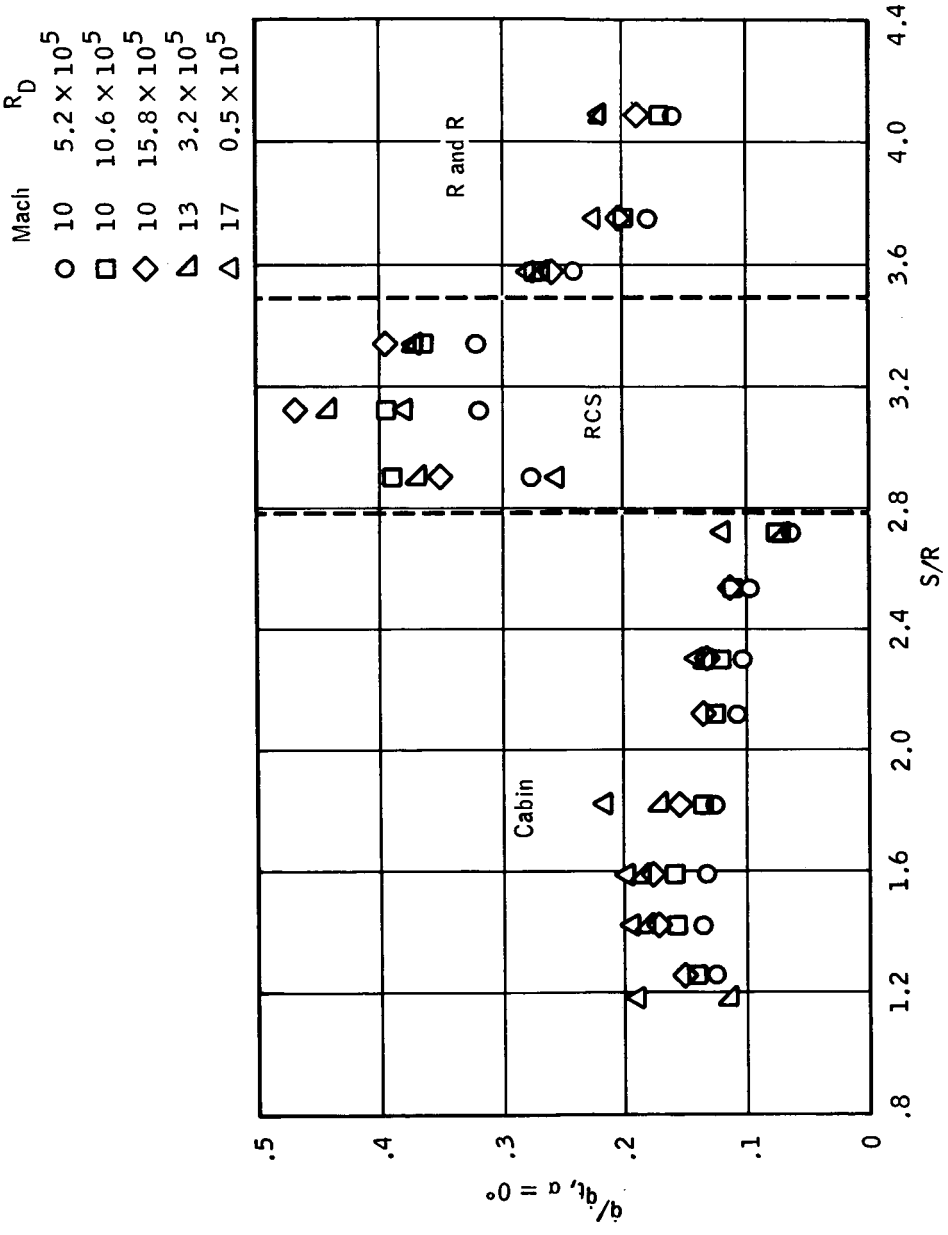

(c) $\alpha = 20°$.

Figure 13.- Concluded.

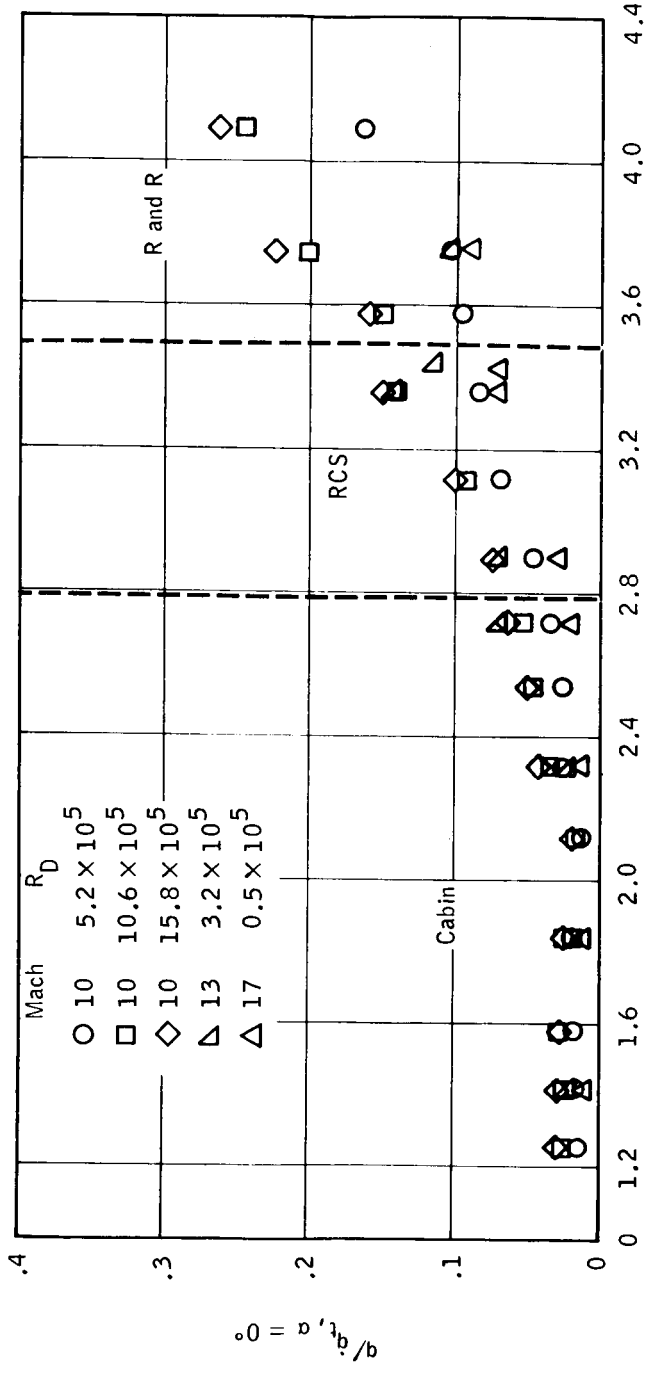

(a) $\alpha = 10°$.

Figure 14.- Wind-tunnel heat-transfer distribution over the leeward side of the reentry configuration afterbody.

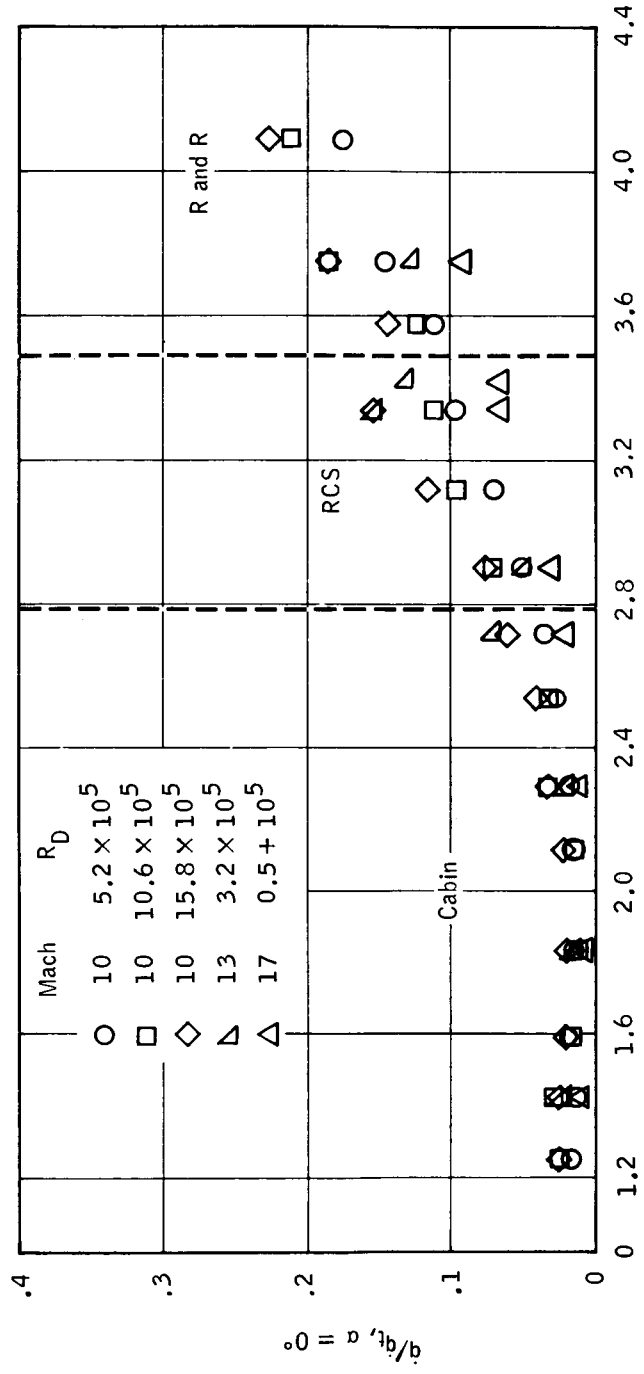

(b) $\alpha = 15°$.

Figure 14.- Continued.

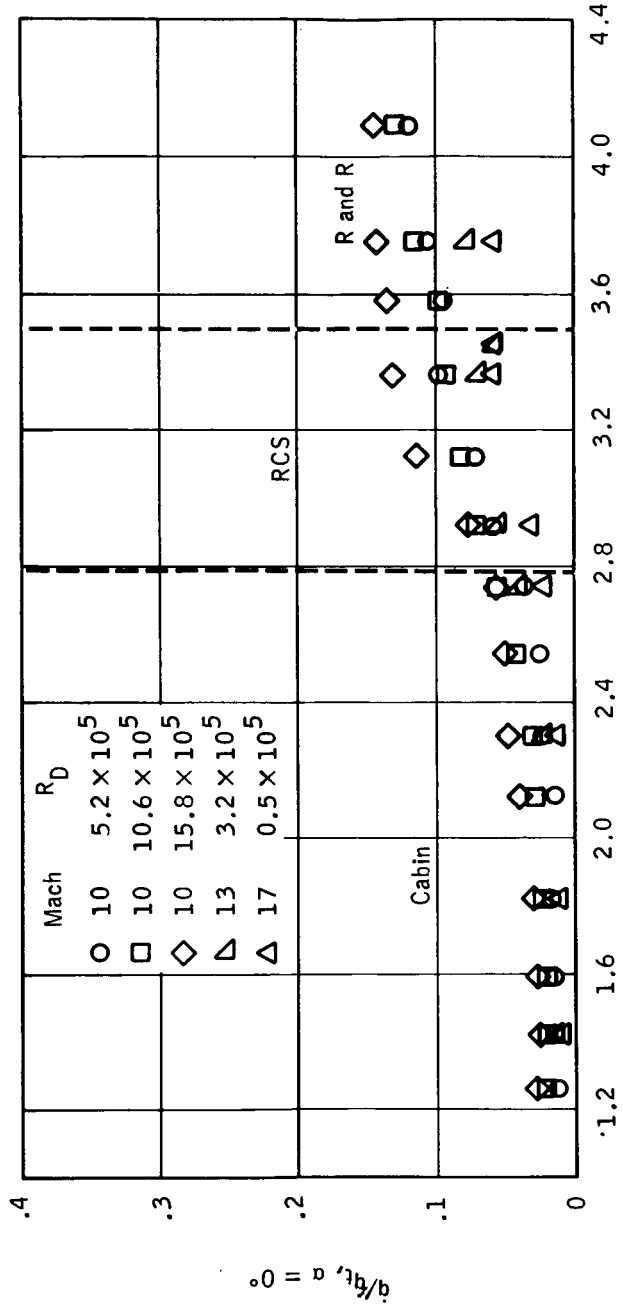

(c) $\alpha = 20°$.

Figure 14. - Concluded.

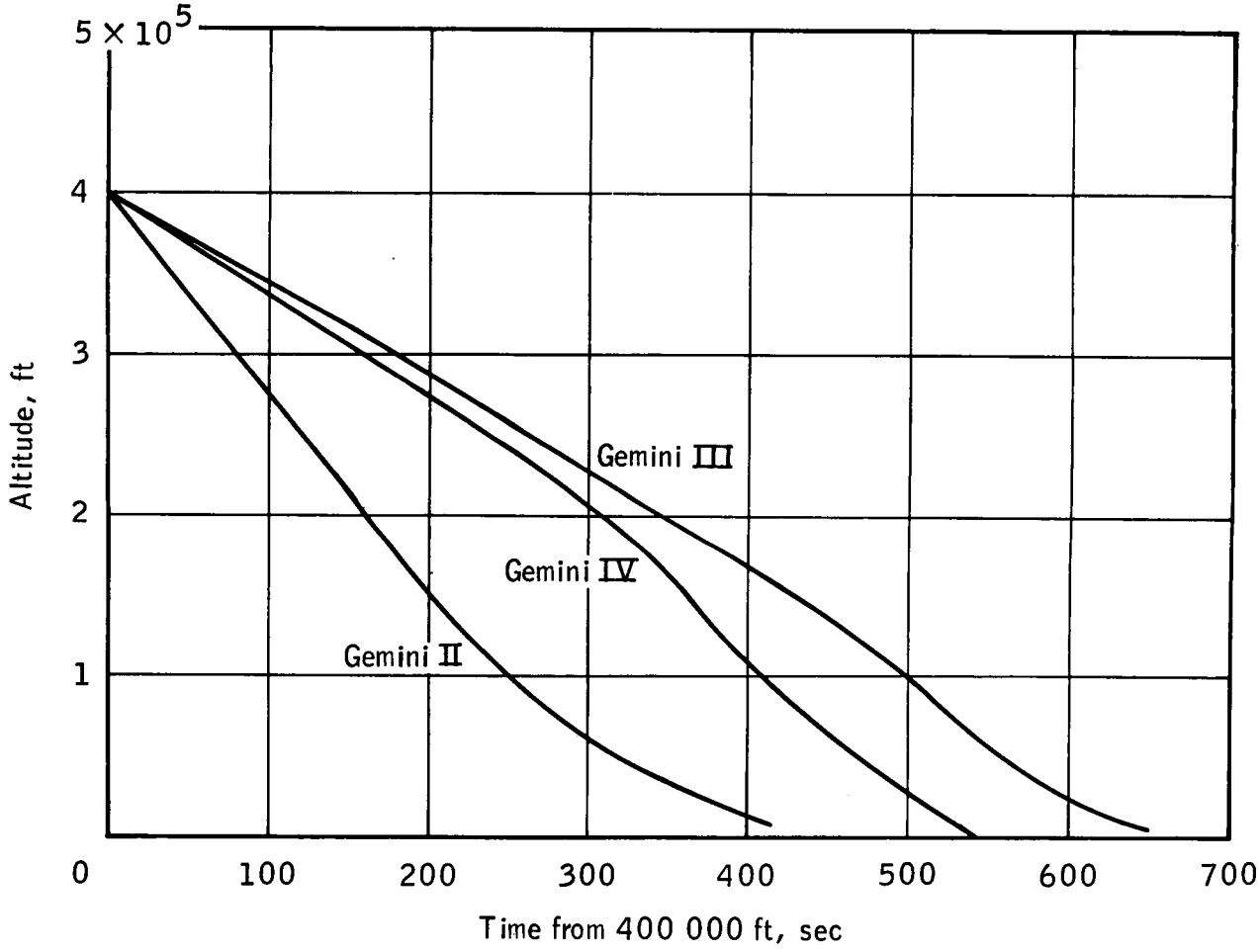

(a) Altitude history.

Figure 15. - Reentry trajectories of the spacecraft of the second, third, and fourth Gemini missions.

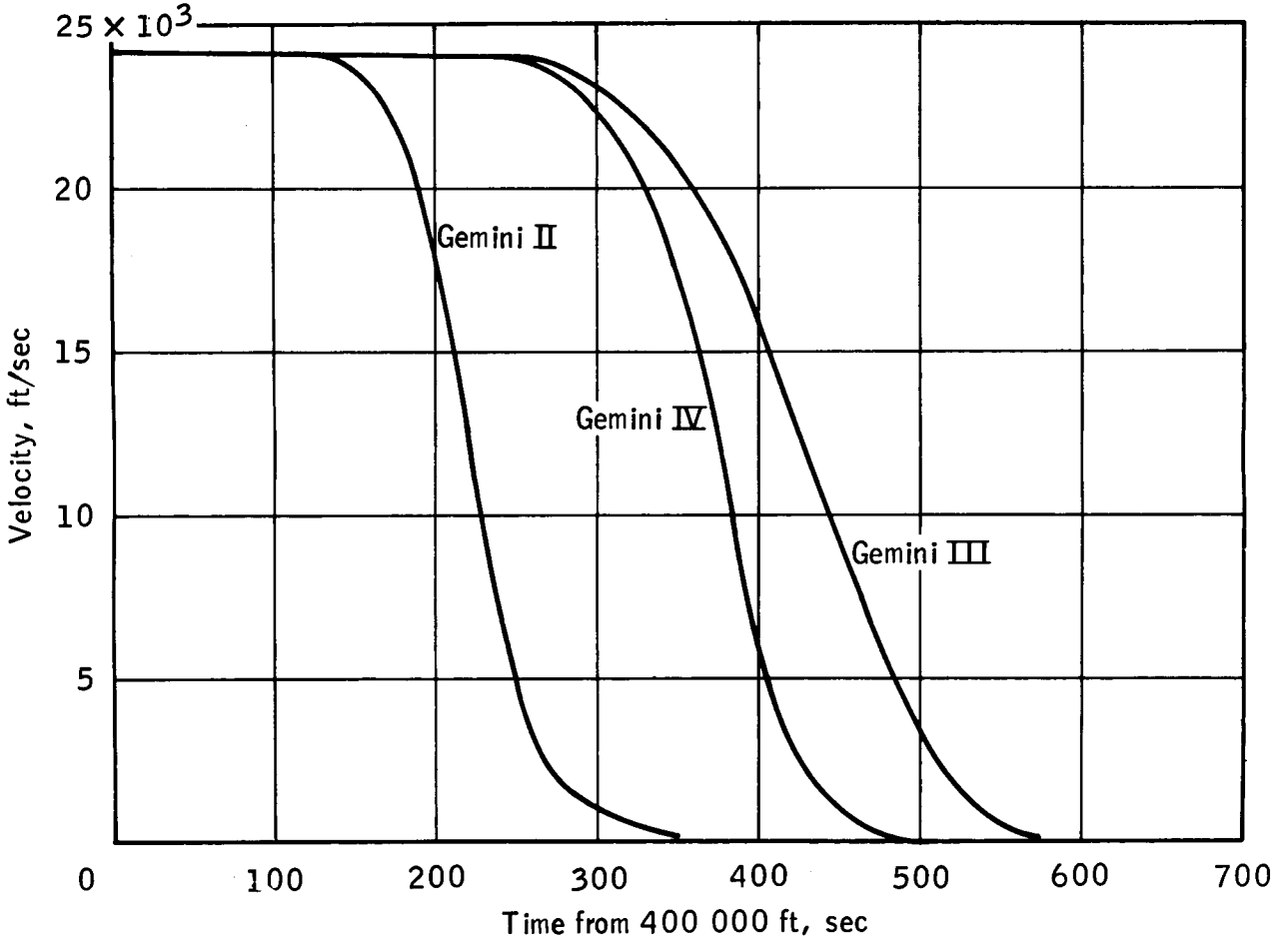

(b) Velocity history.

Figure 15. - Concluded.

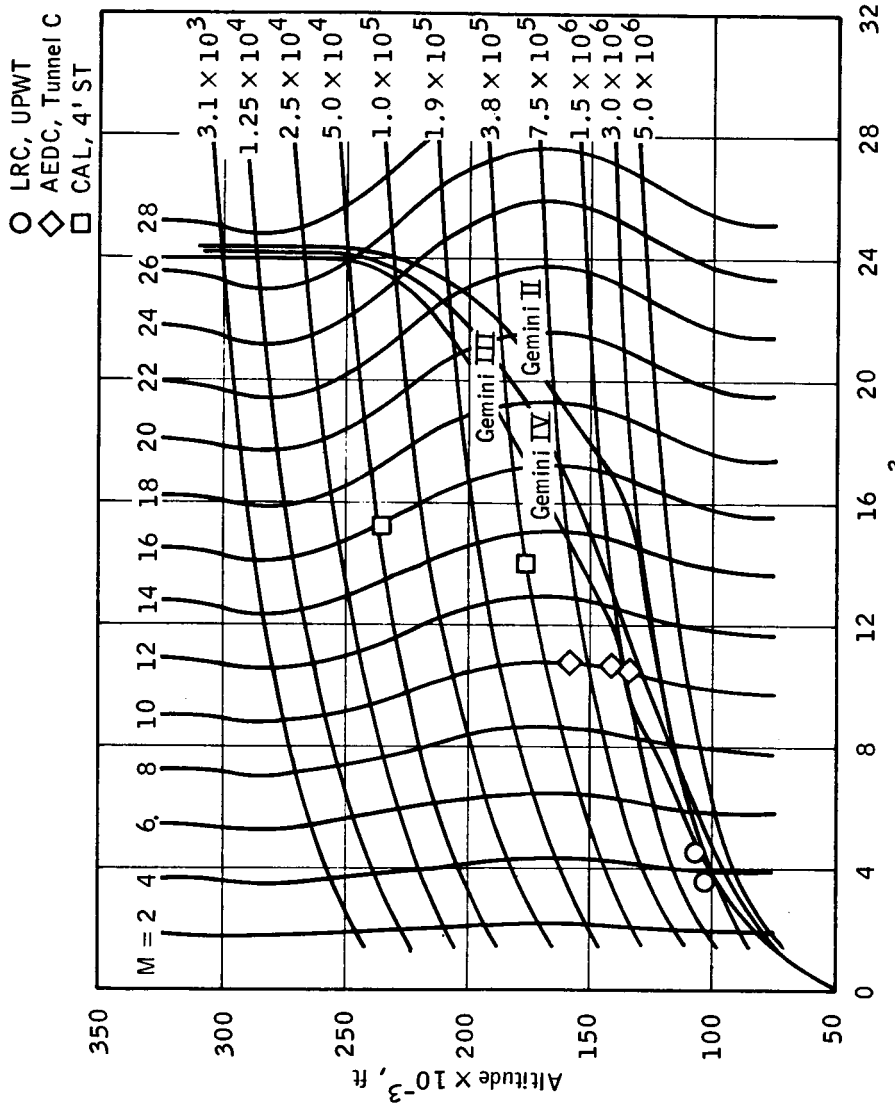

Figure 16. - Gemini reentry aerodynamic environment, 1962 U.S. Standard Atmosphere.

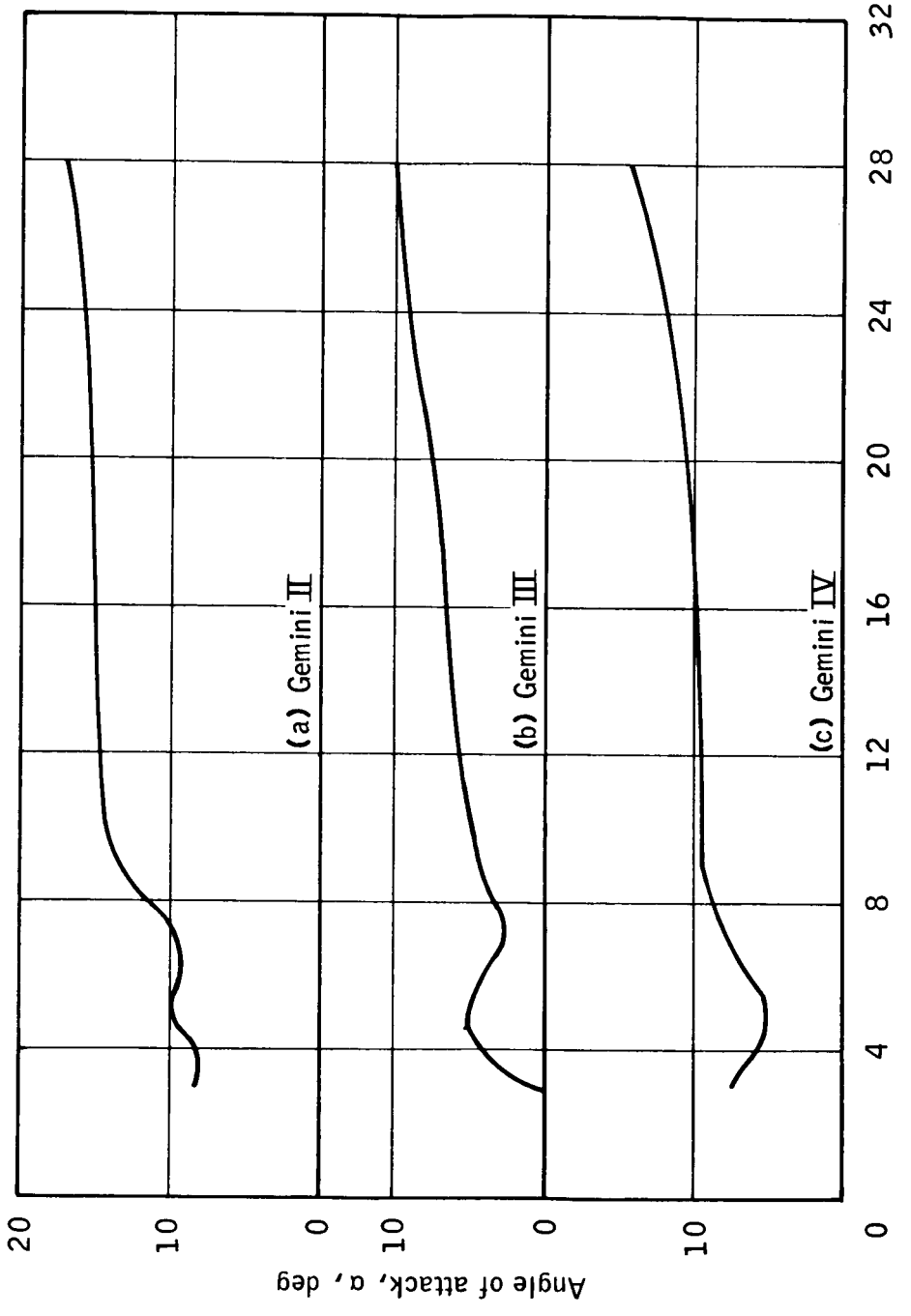

Figure 17.- Reentry angle-of-attack history.

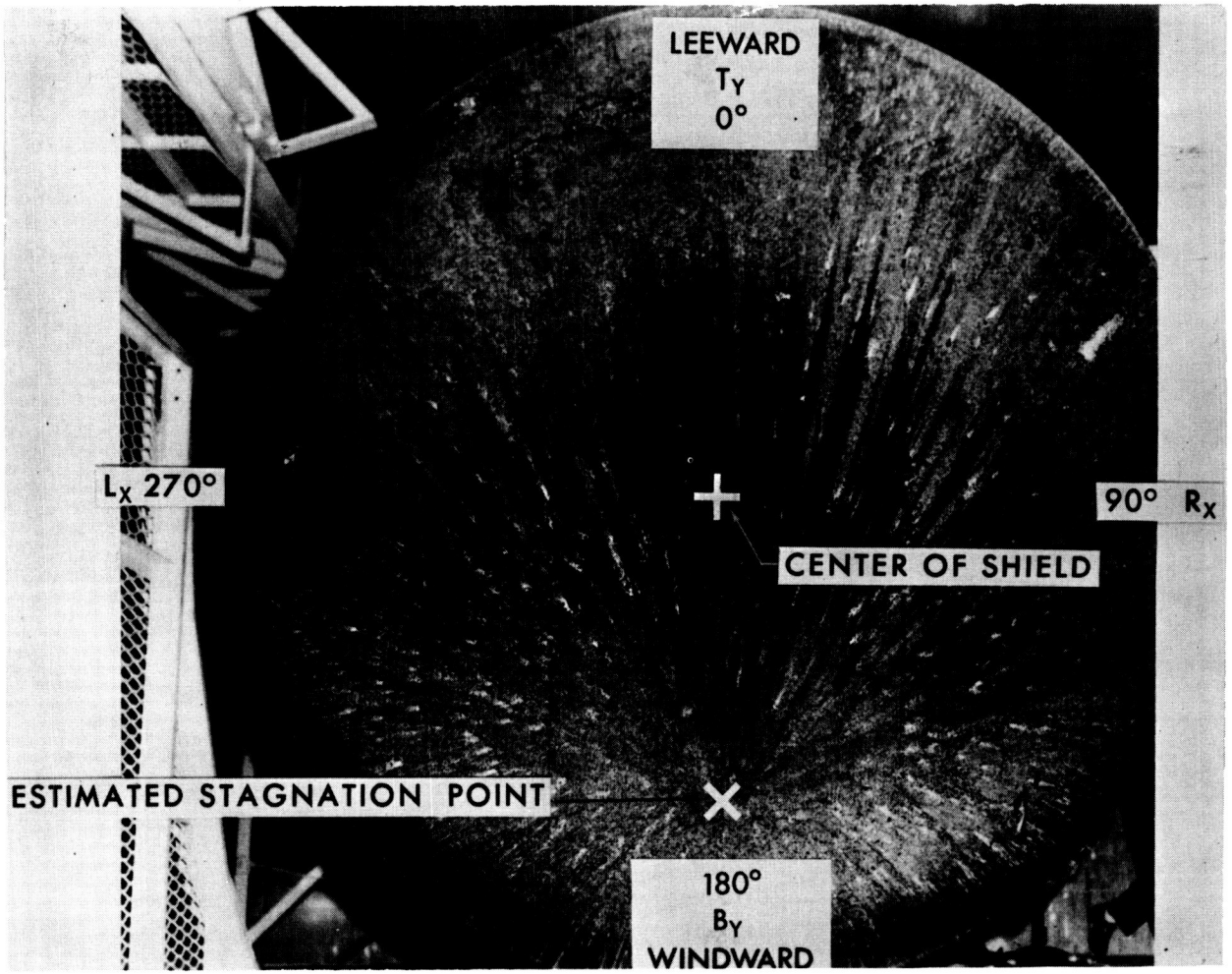

Figure 18. - GT-2 heat shield after flight.

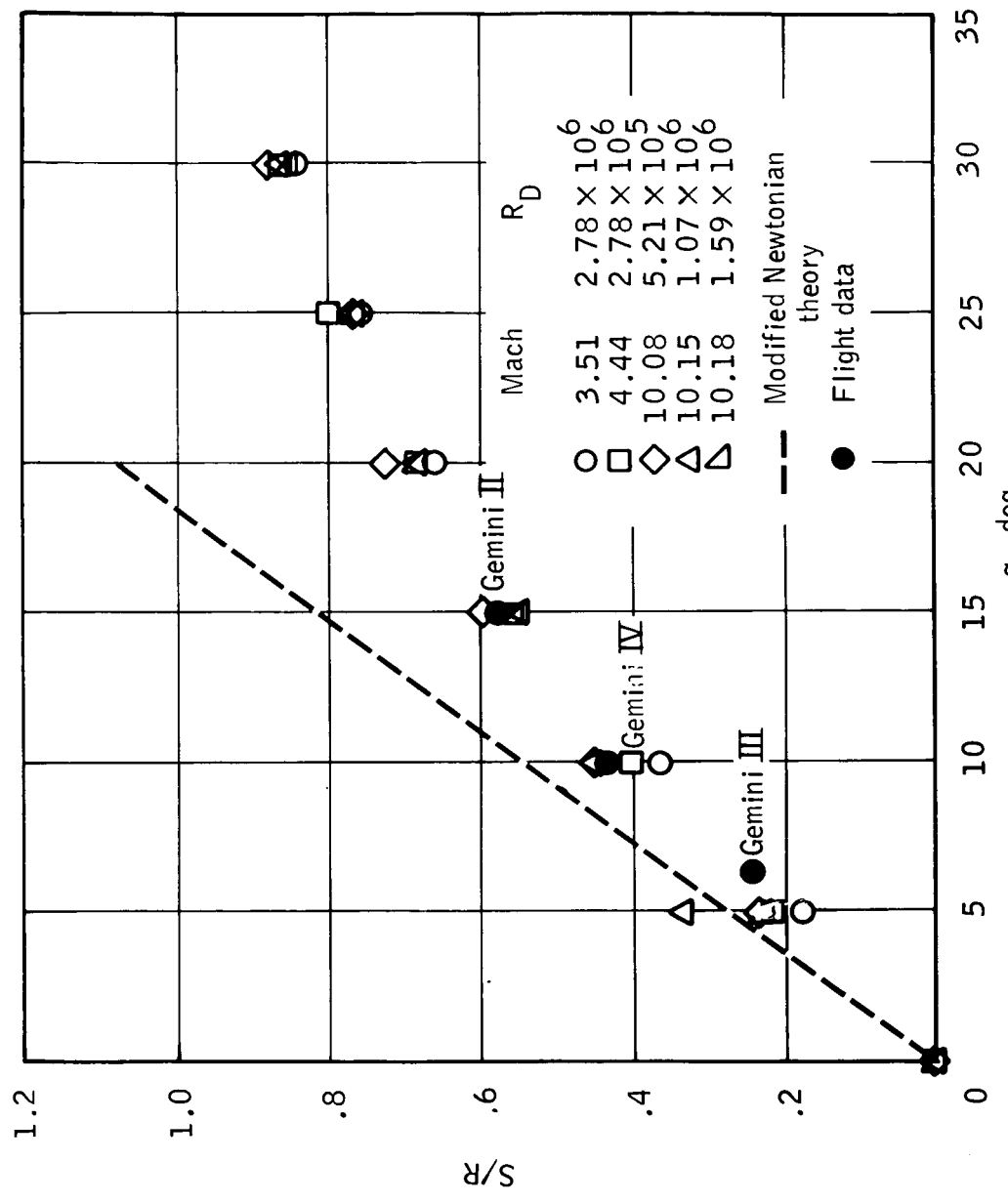

Figure 19.- Comparison of wind-tunnel and flight stagnation-point locations.

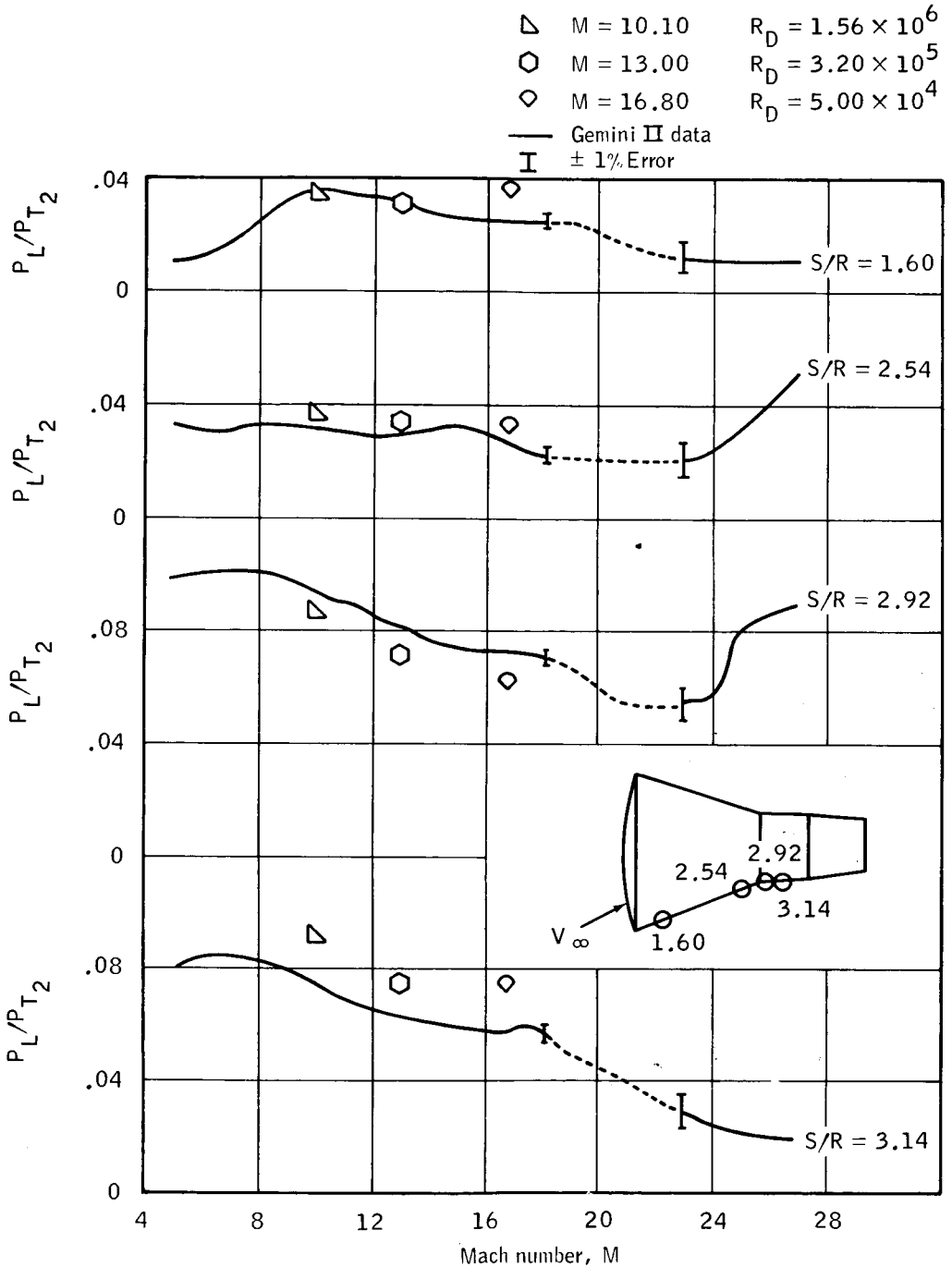

(a) Windward side.

Figure 20. - Comparison of surface pressures measured during flight and in wind-tunnel tests.

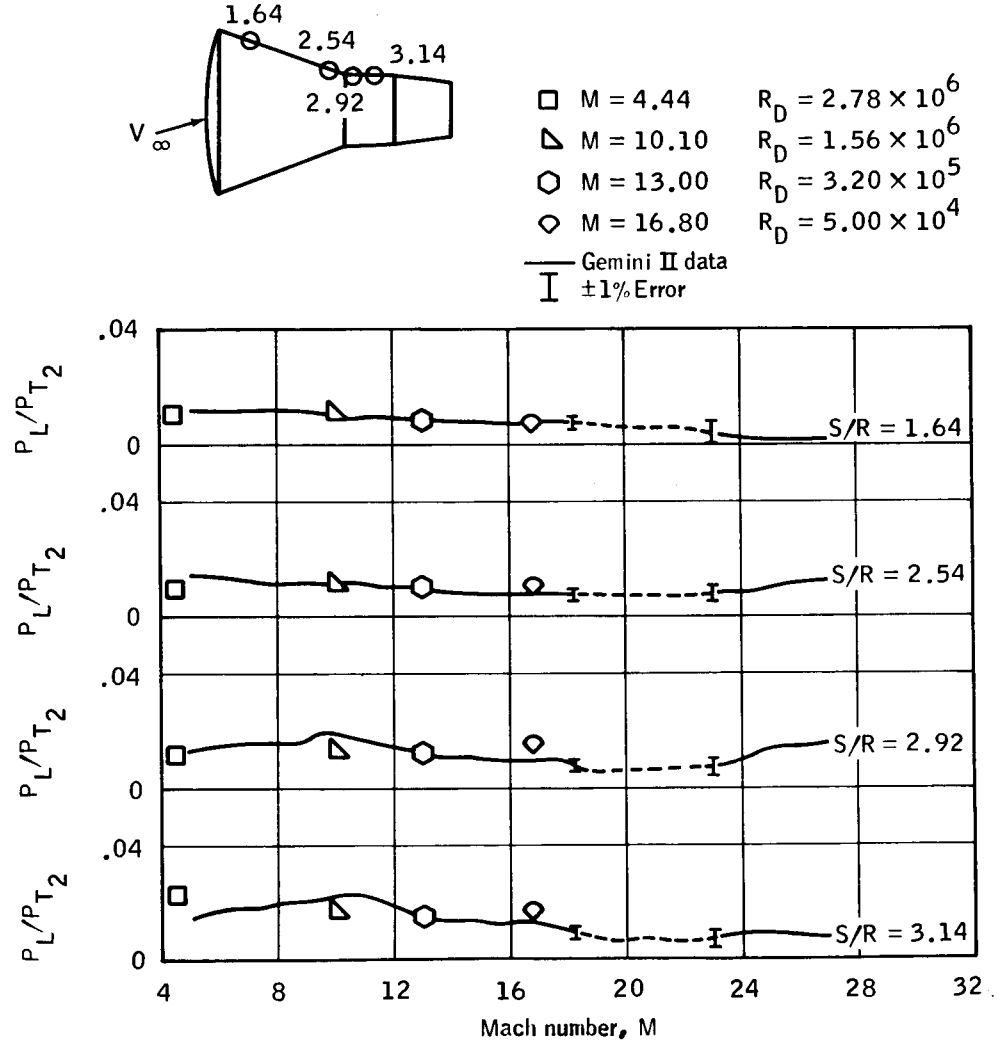

(b) Leeward side.

Figure 20.- Concluded.

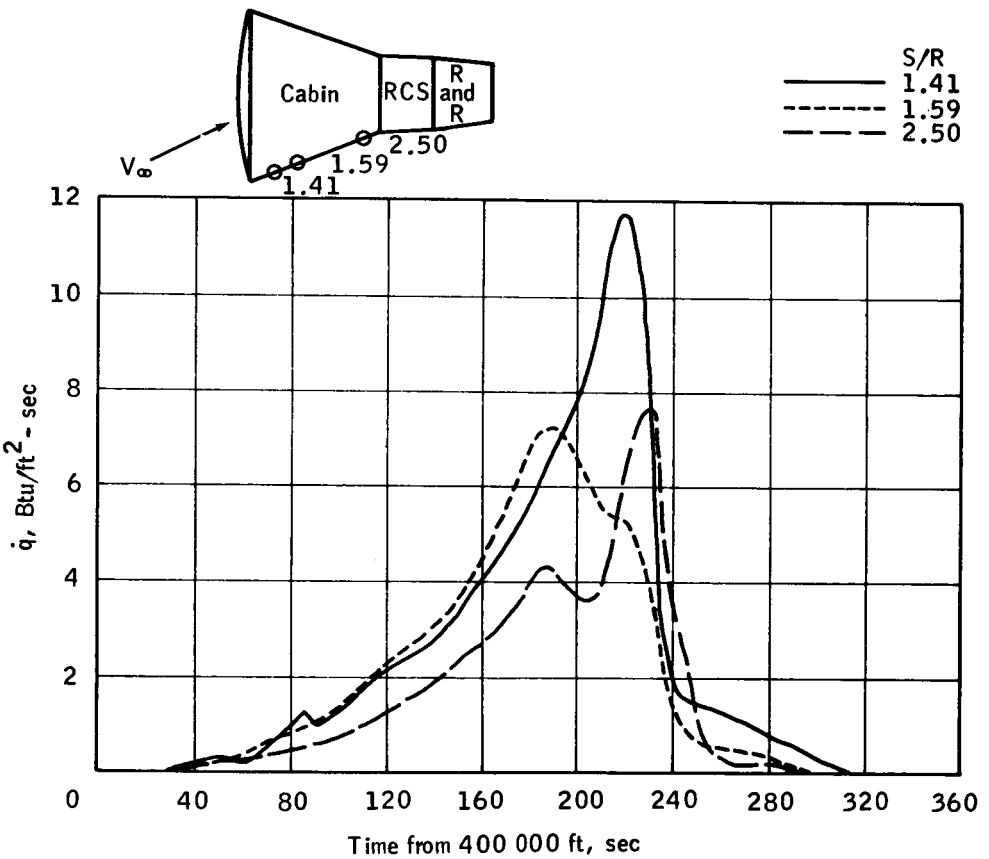

(a) Cabin, windward side.

Figure 21. - Gemini II reentry heating histories.

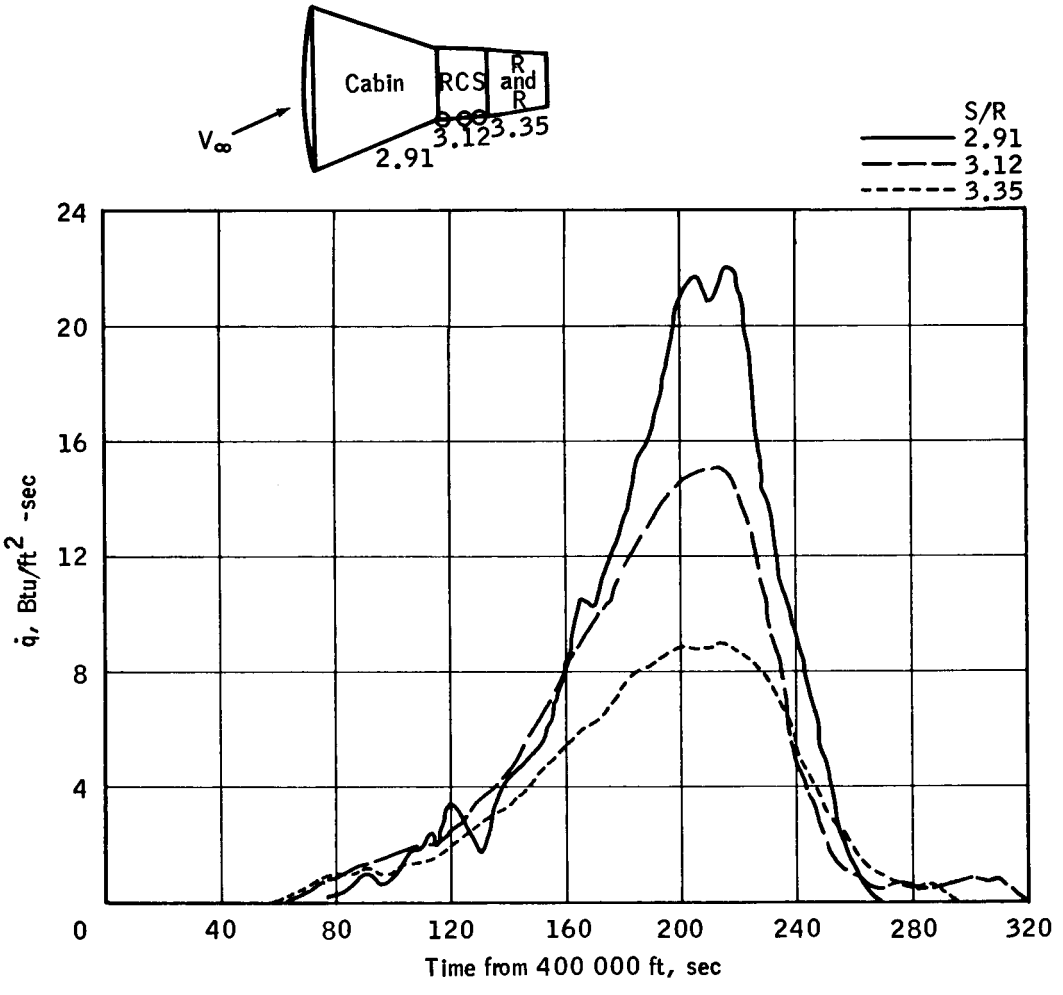

(b) RCS, windward side.

Figure 21.- Continued.

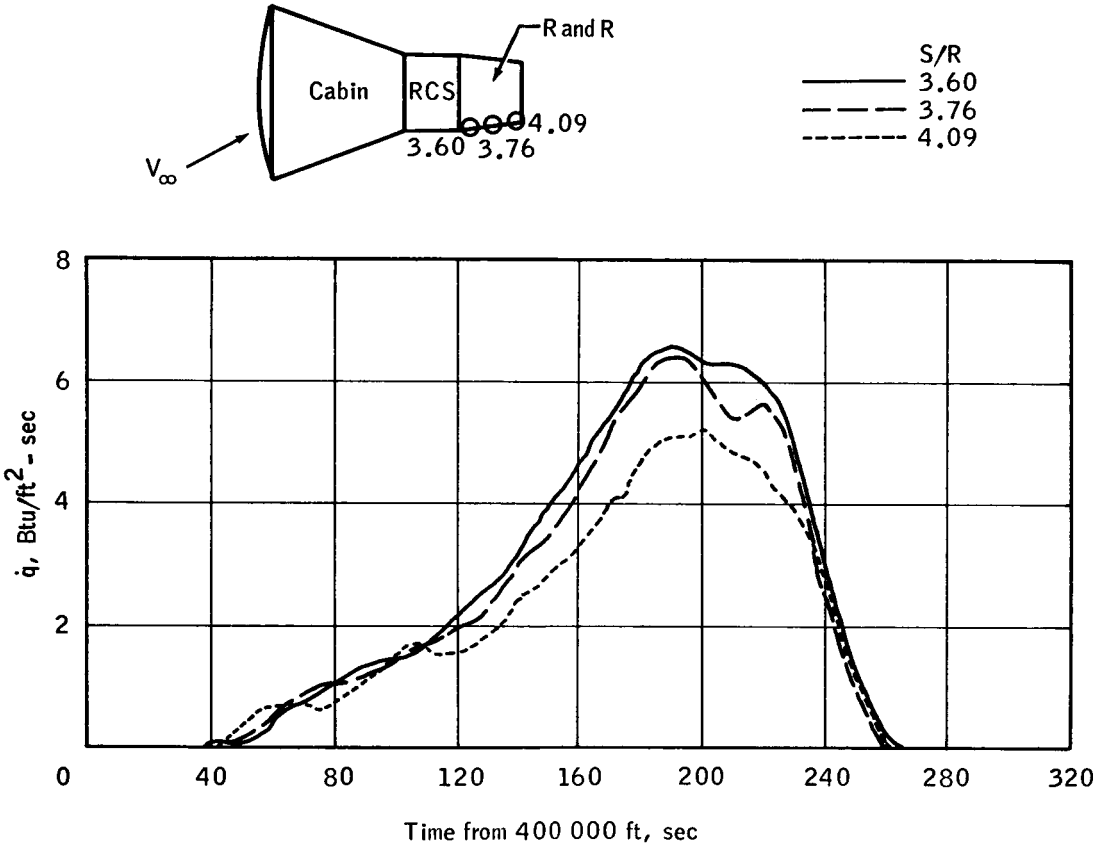

(c) R and R, windward side.

Figure 21. - Continued.

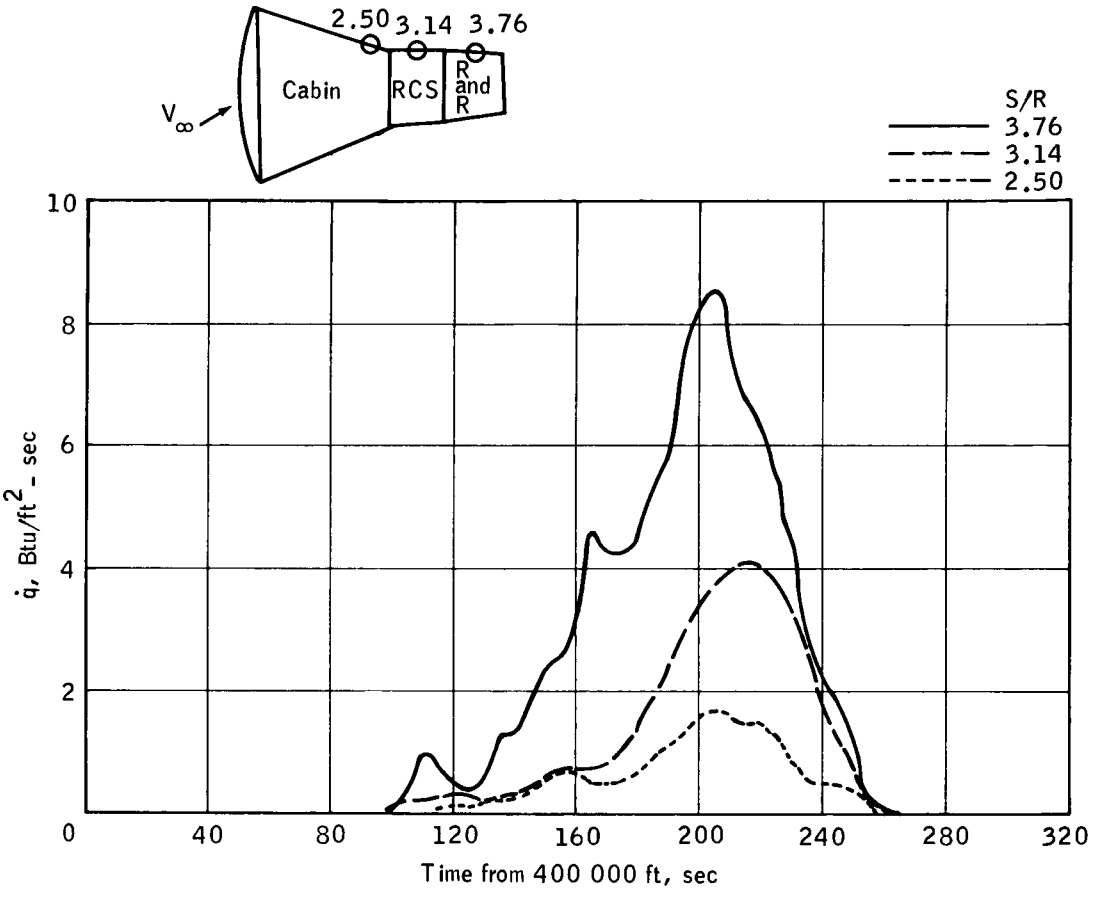

(d) Leeward side.

Figure 21. - Concluded.

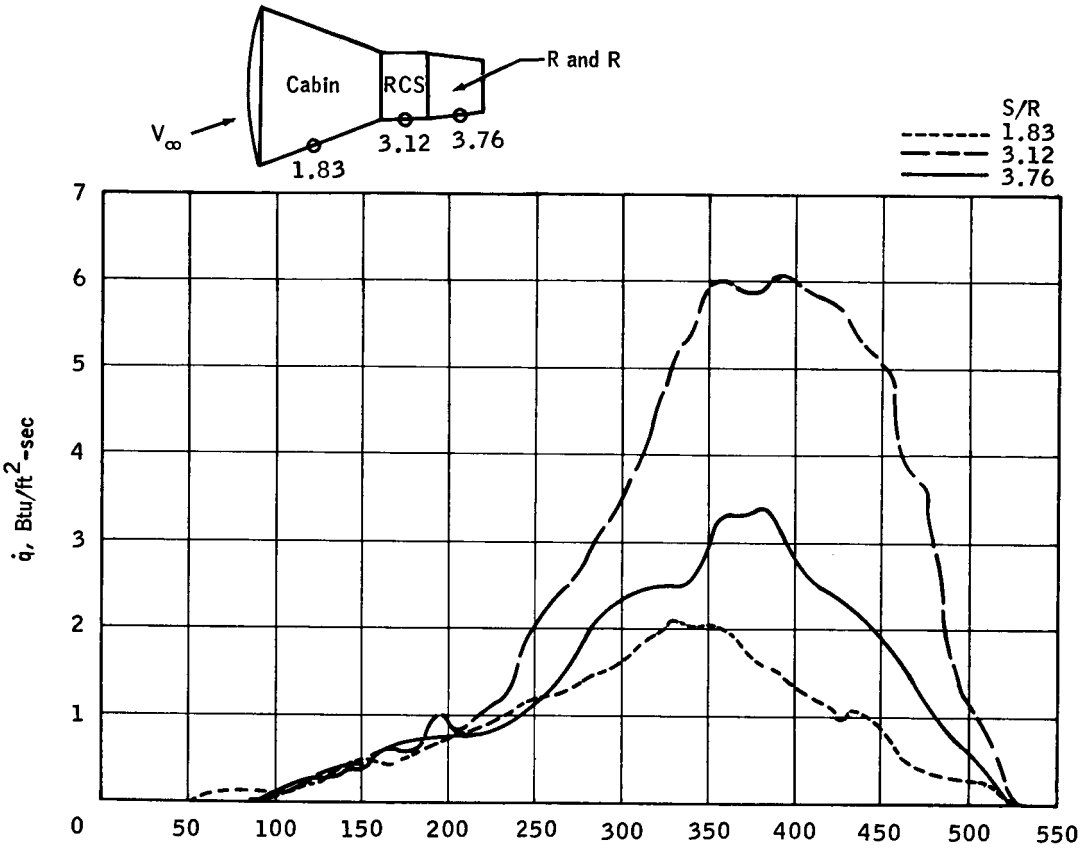

Figure 22. - GT-3 reentry heating-rate histories.

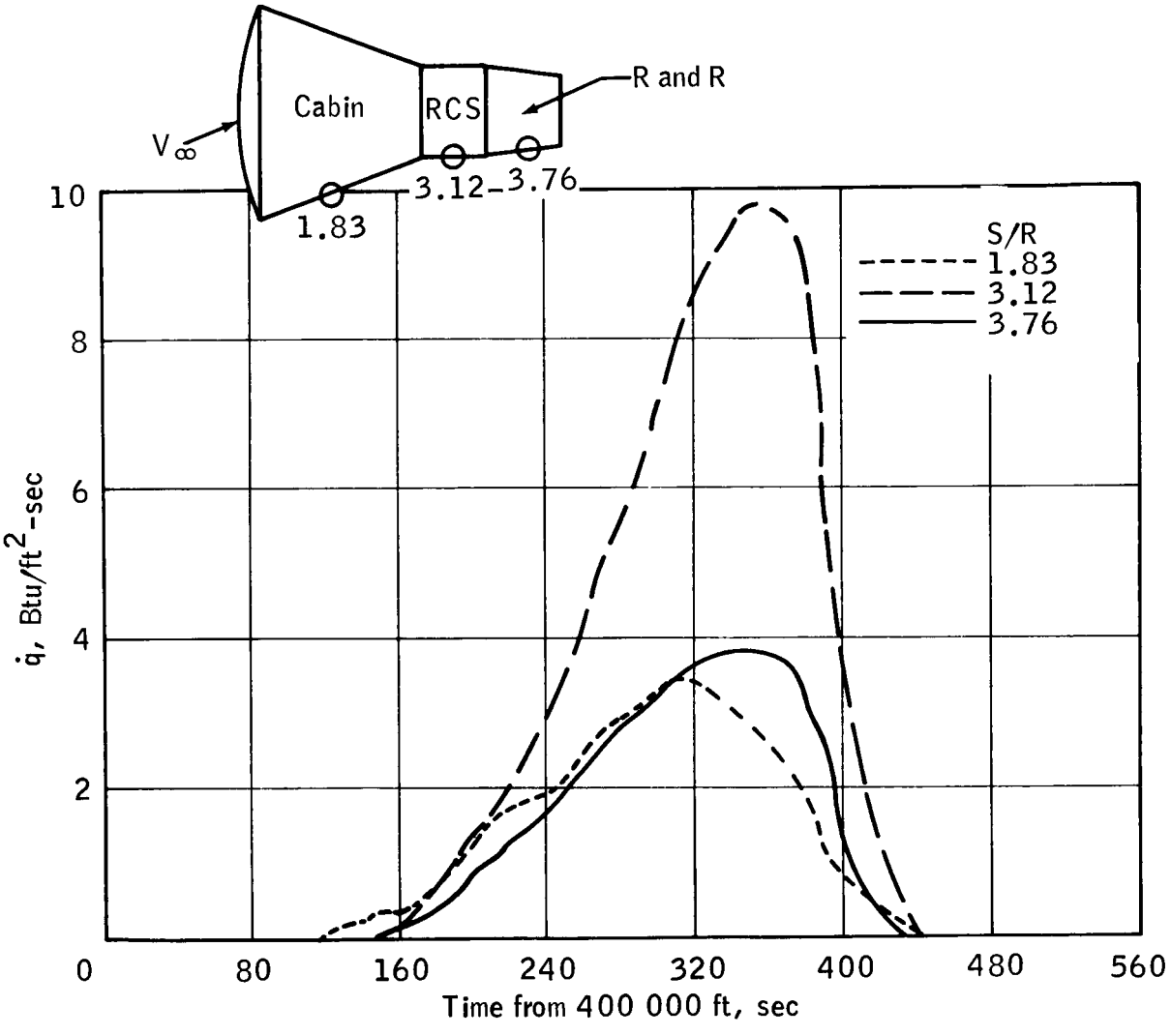

Figure 23. - Gemini IV reentry heating-rate histories.

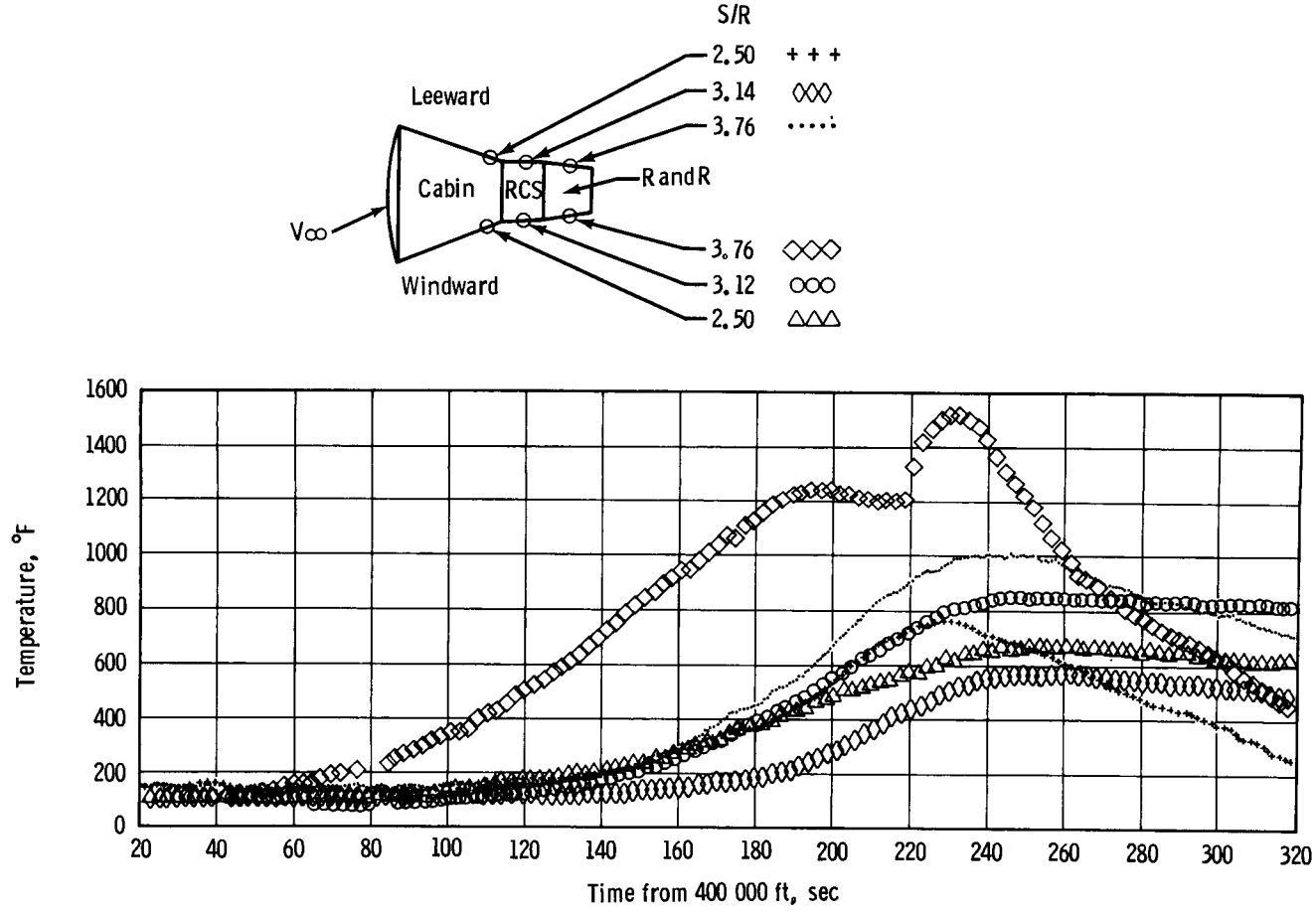

Figure 24. - Gemini II reentry surface thermocouple temperature histories.

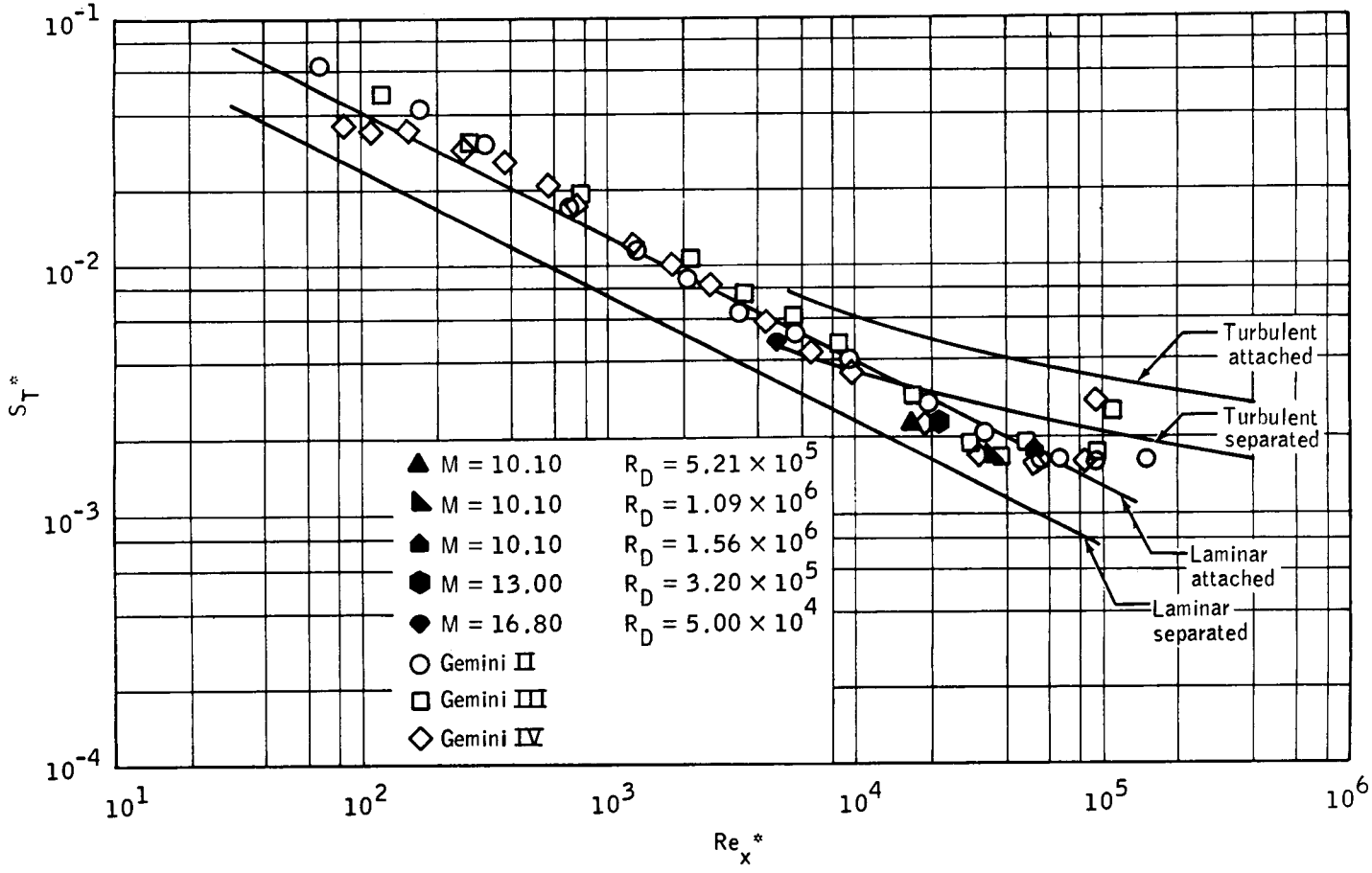

(a) S/R = 1.59.

Figure 25. - Correlation of wind-tunnel and flight heat-transfer data, windward side.

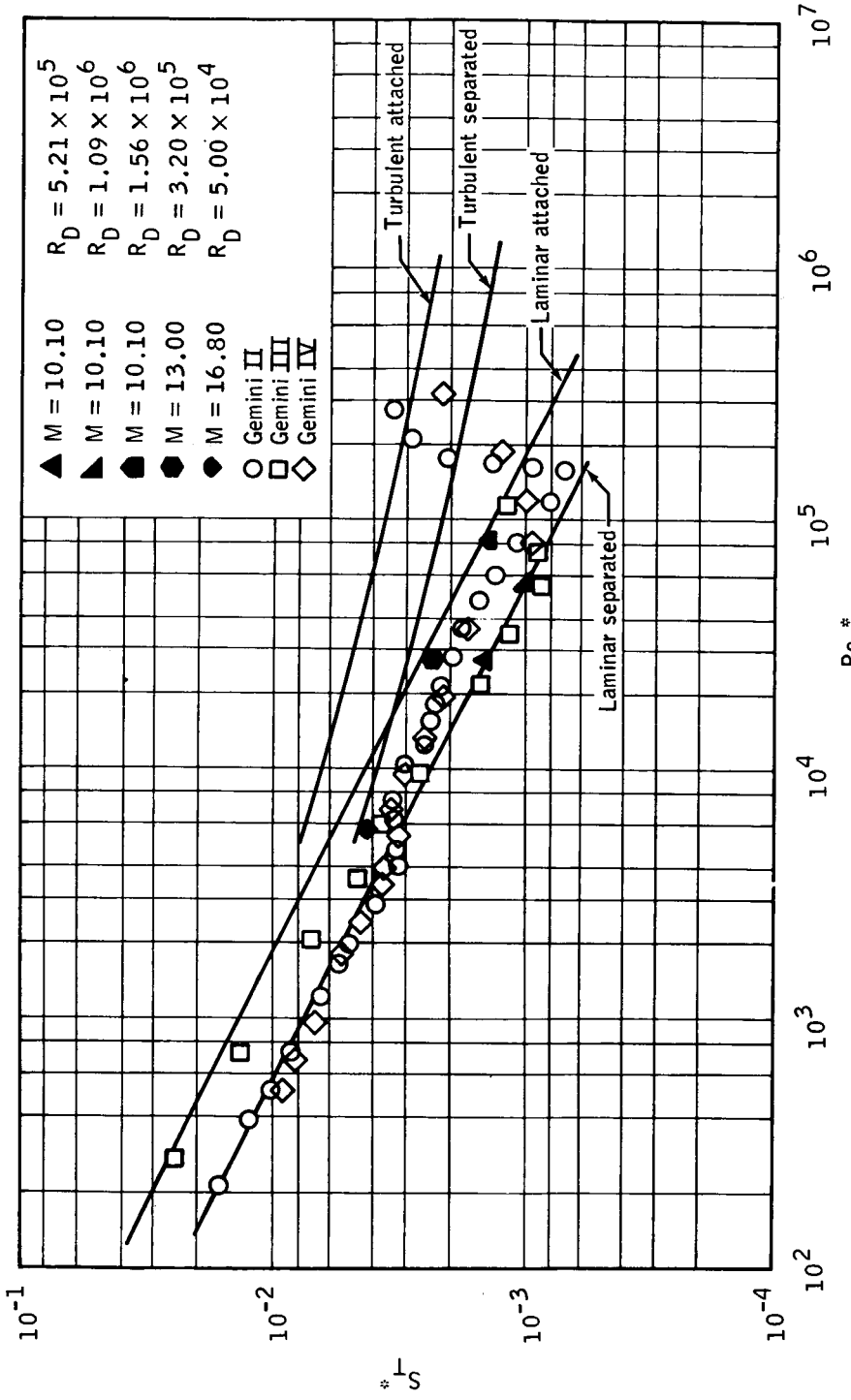

(b) S/R = 2.50.

Figure 25. - Continued.

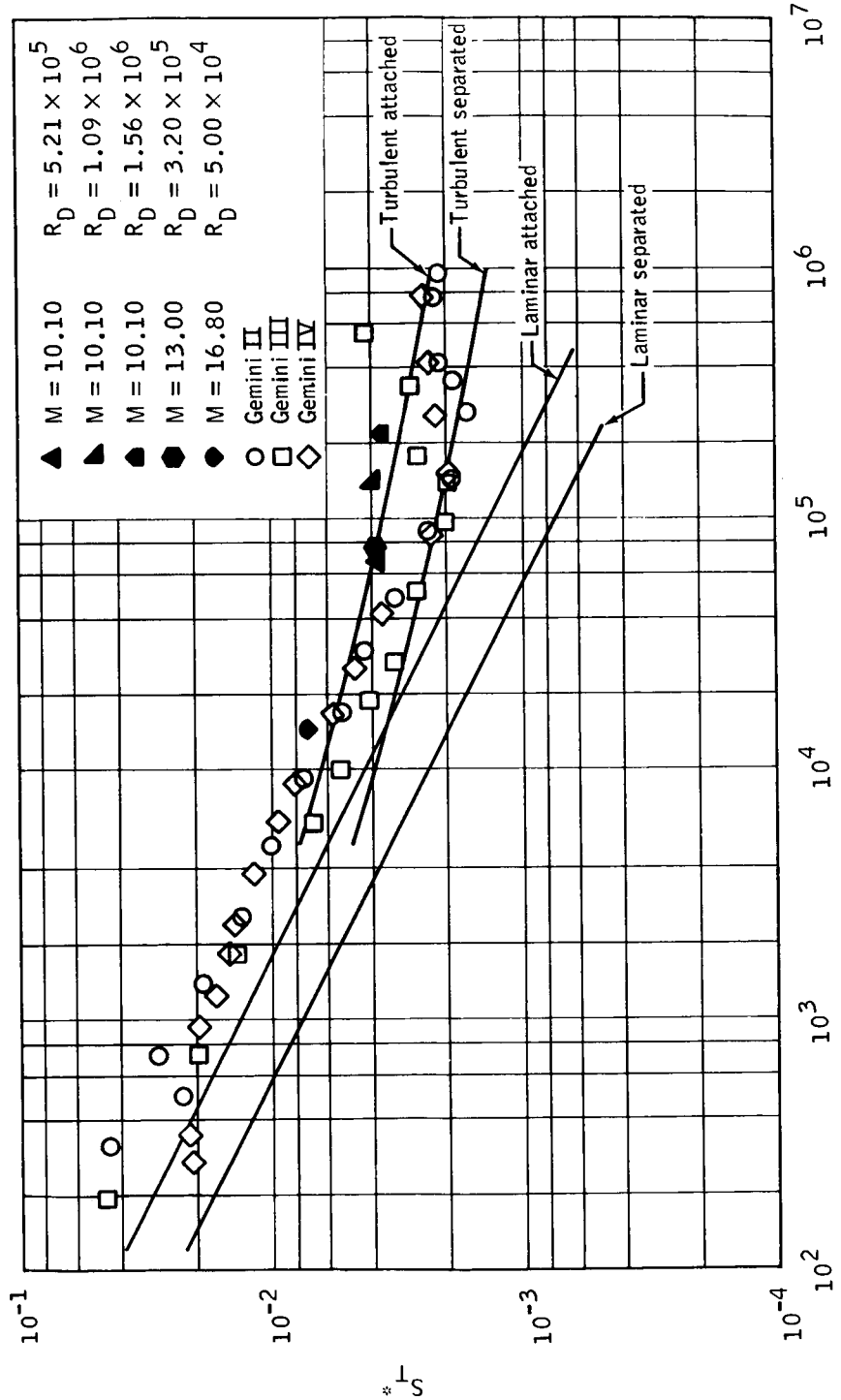

(c) S/R = 3.12.

Figure 25. - Concluded.

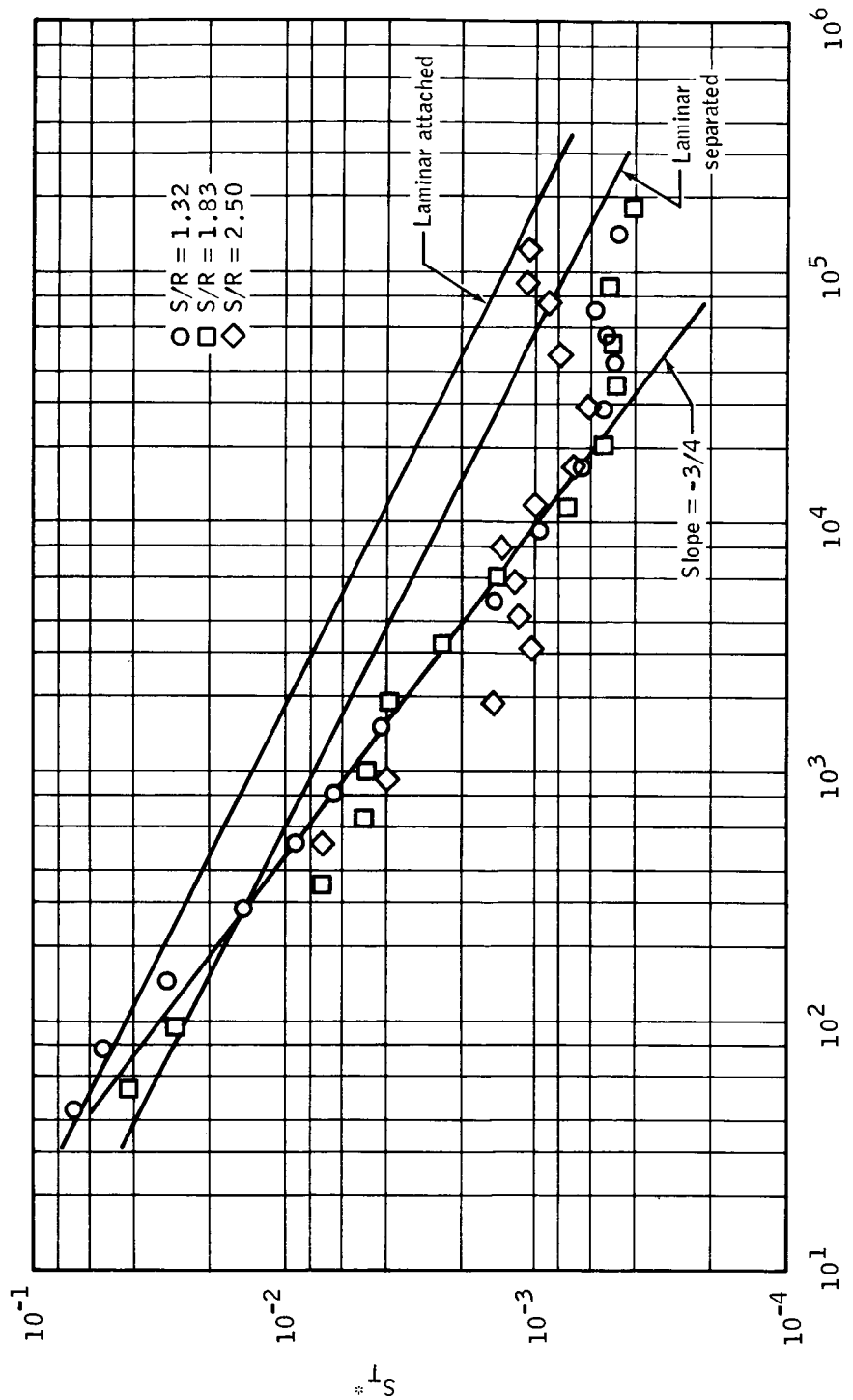

Figure 26.- Correlation of Gemini II leeward side flight data.

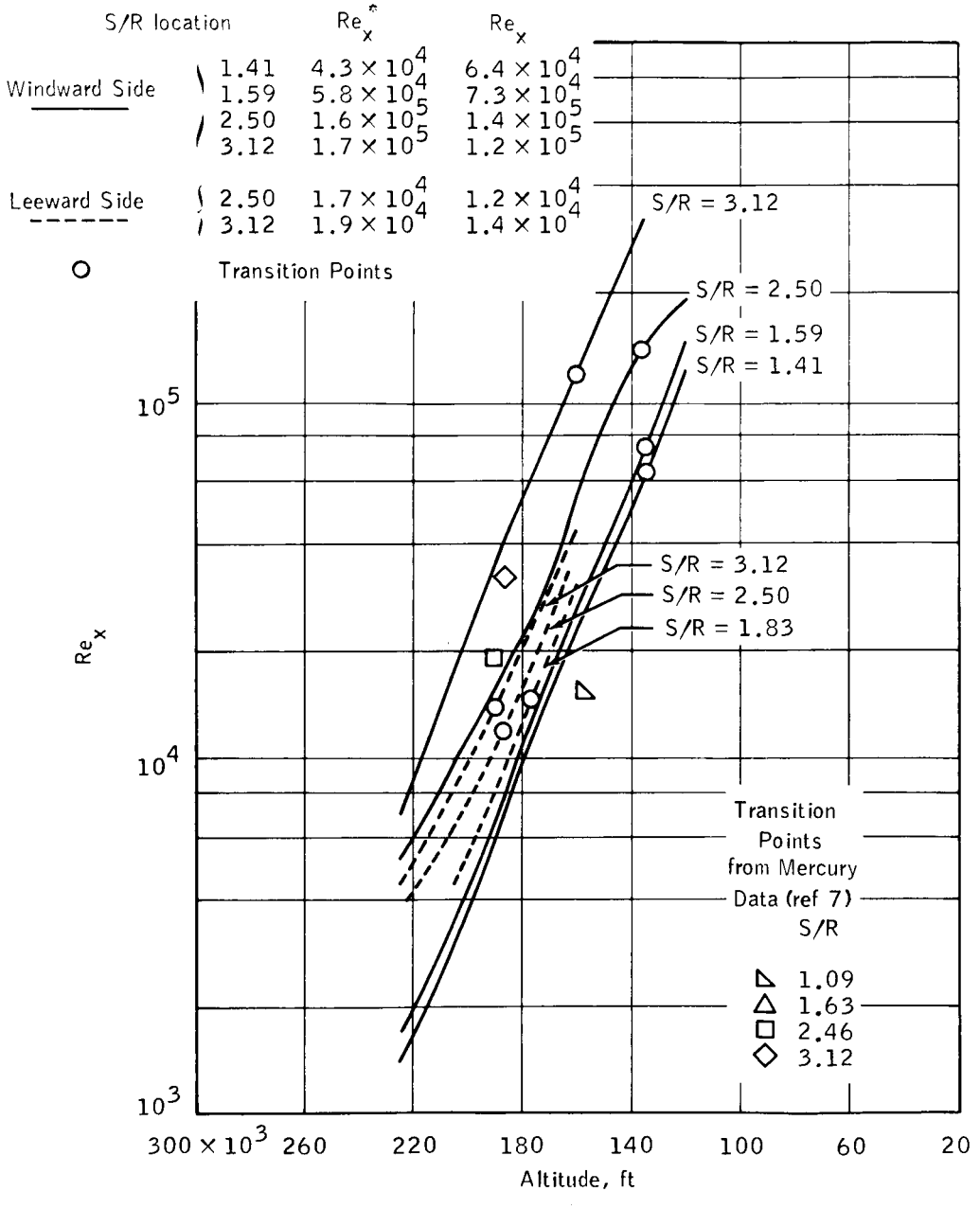

Figure 27. - Effect of altitude on the Reynolds number for the Gemini II reentry.